Competition between Micellization and Liquid-Liquid Phase Separation in Thermosensitive Block Copolymer Solutions

A Doctoral Thesis

by

Chen Kuang

Submitted to

the Graduate School of Science, Osaka University

February, 2020

Acknowledgements

This dissertation contains all my researches under Professor Takahiro Sato's group at department of Macromolecular Science, Graduate School of Science, Osaka University from Oct 2016 to Mar 2020. First of all, I would like to sincere thanks to my supervisor Professor Takahiro Sato. Without his excellent guidance, patience and caring, this dissertation will not be so successfully completed. I also would like to thank Associate Professor Ken Terao for his kind supporting and guidance of my experiments, especially for small angel X-ray scattering measurements.

Secondly, I would like to gratitude to Associate Professor Shin-ichi Yusa at University of Hyogo, for his kind supporting of polymer samples and kind revision of the publication as a co-author (Chapter III). I also would like to thank Dr. Rintaro Takahashi at University of Kitakyushu, for his supporting of PNIPAM samples and very important advices about my research.

Next, I would like to thank all members in Sato laboratory for their very kind helps, whatever taught my experimental instruments or gave me critical questions and comments. The all are affecting me and this dissertation.

At last, I would like to express my deep thanks and loves for my parents, for their understanding and financial support of my Ph.D career. I also would like to thank my wife, for her long time supporting and helps when I faced difficulties and challenges.

Chen Kuang

Contents

Chapter I

General Introduction

I-1. Polymer Self-Assemblies Used in the Field of Nano-Technology

In biological systems, molecular assemblies of proteins,[1-3] nucleic acids,[4,5] polysaccharides,[6,7] and lipids[8-10] play important roles to engage in life activities. Inspired by these life systems, polymer scientists recently intend to apply molecular assembly systems of synthetic polymers as nano-carriers,[11,12] nano-reactors,[13-15] and so on. Drug delivery systems utilizing amphiphilic block copolymers are typical examples of such intentions.[16]

It is known that amphiphilic block copolymer chains can form the spherical micelles, cylindrical micelles, or disk-like micelles (vesicles) in selective solvents,[17] while solvophobic homopolymer chains form spherical droplets in the poor solvents (cf. Figure 1-1).[18,19] They are referred to as polymer self-assemblies, because these structures are spontaneously constructed by inter-chain attractive interactions in solution.

It is very important to control the structure and size of polymer self-assemblies in order to apply them as nano-carriers and nano-reactors in the field of nanotechnology.[20-23] For example, drug delivery systems carrying anti-cancer drugs can accumulate in tumor tissues much more than in normal tissues by controlling the nano-carrier size.[24] The size of the polymer micelles is usually an order of nanometers to sub-microns. The spherical droplet size of solvophobic homopolymers depends on the polymer-solvent system, but in some cases the droplets stop growing at some stage and possess the size of sub-microns order. However, polymer self-assemblies possess size or aggregation number distributions intrinsic to the assembly morphology. We have to know the intrinsic distribution of the aggregation number for each

polymer self-assembly in solution to control the polymer assembly size.

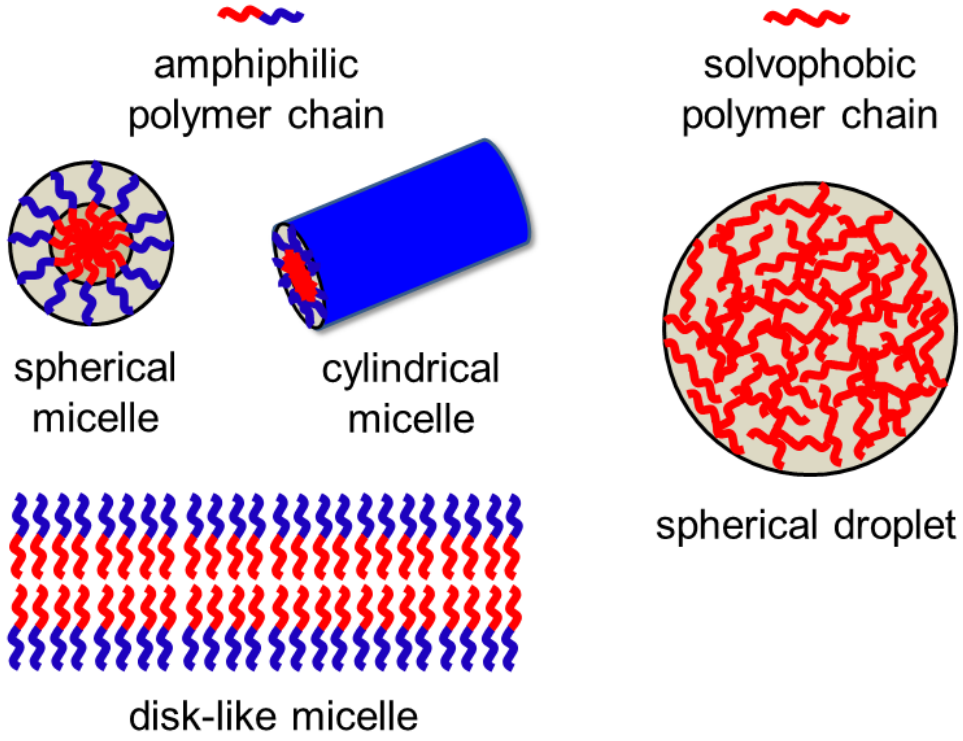

Figure I-1. Schematic diagrams of the spherical micelle, cylindrical micelle, or disk-like micelle formed by amphiphilic polymer chains, as well as of the spherical droplet formed by solvophobic polymer chains in the solvent.

I-2. Distributions of the Aggregation Number for Polymer Self-Assemblies in Solution

The aggregation number distribution of polymer self-assemblies in solution is generally determined by the following dissociation-association equilibrium.[17,25]

$$m\mathrm{M} \rightleftharpoons[K_m] \mathrm{M}_m \qquad \text{(I-1)}$$

where m is the aggregation number, M and M_m denote the unimer and m-mer, respectively, and K_m is the association constant. In the system in dissociation-association equilibrium, the following equation holds

$$m\mu_1 = \mu_m \tag{I-2}$$

with μ_1 and μ_m being the chemical potentials of M and M_m in solution, respectively.

If the solution is sufficiently dilute and the interactions between solute molecules are negligible, the chemical potential of the m-mer is generally given by:

$$\mu_m = \mu_m^\circ + RT \ln\left(\frac{\phi_m}{m}\right) \tag{I-3}$$

Here, $\mu_m°$ is the standard chemical potential of M_m, ϕ_m is the volume fraction of M_m in the solution, and RT is the gas constant multiplied by the absolute temperature. This equation is substituted into eq I-2, we have the equation for K_m in the form

$$K_m \equiv \frac{\phi_m}{\phi_1^m} = m \exp\left(\frac{m\mu_1^\circ - \mu_m^\circ}{RT}\right) \tag{I-4}$$

where ϕ_1 is the volume fraction of M. From eq I-4, it can be shown that for large m, ϕ_m abruptly increases when the total polymer volume fraction exceeds the critical volume fraction

$$\phi_{\mathrm{CMC}} = K_m^{-2/m} \tag{I-5}$$

Thus, this critical volume fraction is referred to as the critical micelle concentration (cmc). The distribution function of the aggregation number for the polymer self-assembly or the polymer micelle in solution is determined by the dependence of $\mu_m°$ on m.

When m amphiphilic block copolymer chains assemble to form a spherical micelle, m solvophobic block chains gain the Gibbs energy proportional to m, but the repulsive pair interaction proportional to m^2 provides the Gibbs energy loss. As the result, $\mu_m°$ can be written in the form

$$\mu_m^\circ = gm + g_e m^2 \tag{I-6}$$

with two proportional coefficients g and g_e.

When m amphiphilic block copolymer chains assemble to form a cylindrical micelle, m solvophobic block chains gain the Gibbs energy proportional to m, and the cylinder ends destabilize the Gibbs energy g_e (a constant). As the result, μ_m° can be written in the form

$$\mu_m^\circ = gm + g_e \tag{I-7}$$

Furthermore, when m amphiphilic block copolymer chains assemble to form a disk-like micelle, m solvophobic block chains gain the Gibbs energy proportional to m, and the edge of the disk destabilize the Gibbs energy which is proportional to $m^{1/2}$. As the result, μ_m° can be written in the form

$$\mu_m^\circ = gm + g_e m^{1/2} \tag{I-8}$$

Finally, when m solvophobic homopolymer chains assemble to form a spherical droplet, m solvophobic chains gain the Gibbs energy proportional to m, and the spherical surface of the droplet destabilize the Gibbs energy which is proportional to $m^{2/3}$. Thus, μ_m° can be written as

$$\mu_m^\circ = gm + g_e m^{2/3} \tag{I-9}$$

These equations I-6–9 for μ_m° are inserted into eq I-4 to obtain[25]

$$\phi_m = \begin{cases} e^{g_e m_0^2}\, m \exp\left[-g_e \left(m - m_0\right)^2\right] & \left(\text{spherical micelle}\right) \\ m\, e^{-g_e} \left(\phi_1\, e^{g_e}\right)^m & \left(\text{cylindrical micelle}\right) \\ m\left(\phi_1\, e^{g_e}\right)^m \exp\left(-g_e m^{1/2}\right) & \left(\text{disk-like micelle}\right) \\ m\left(\phi_1\, e^{g_e}\right)^m \exp\left(-g_e m^{2/3}\right) & \left(\text{spherical droplet}\right) \end{cases} \tag{I-10}$$

with m_0 [$\equiv (1 + g_e^{-1} \ln \phi_1)/2$] being the optimum aggregation number for the spherical micelle. These ϕ_m provides the distribution function of the aggregation number for the polymer assemblies.

The above distribution for the cylindrical micelle is the most probable distribution, identical with the molecular weight distribution of polycondensates.[26] It is known that this distribution gives us the ratio of the weight-average to number-average aggregation numbers m_w/m_n to be 2, when $\phi_1 \exp(g_e)$ approaches to unity. Figure I-2 shows the distribution functions calculated by eq 1.10 with $\phi_1 \exp(g_e) = 0.999$. The distribution for the spherical micelle given by eq I-10 is much sharper than the most probable distribution, as shown in Figure I-3. On the other hand, in a dilute solution with $\phi_1 \leq 0.01$, large disk-like micelles (or the vesicles) and spherical droplets are not formed, if $\phi_1 \exp(g_e) < 1$ in eq I-10. We have to choose $\phi_1 \exp(g_e)$ larger than unity, but this choice gives us the divergence of ϕ_m at large m, as shown in Figure I-3. Thus, there are no thermodynamically stable aggregation number distributions for large disk-like micelles (or the vesicles) and spherical droplets.

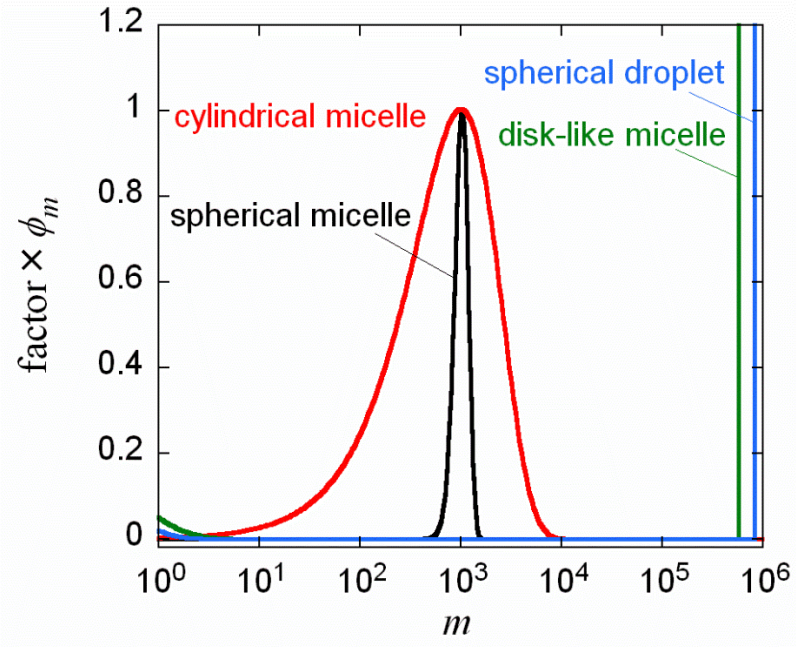

Figure I-2. Aggregation number distributions of the spherical micelle ($m_0 = 10^3$, $g_e = 2 \times 10^{-5}$, cylindrical micelle [$\phi_1 \exp(g_e) = 0.999$], disk-like micelle [$\phi_1 \exp(g_e) = 1.006$], and spherical droplet [$\phi_1 \exp(g_e) = 1.05$] in the solution with $\phi_1 = 0.01$, calculated by eq I-10.

When a dilute homopolymer solution is brought into the two-phase region from the one-phase region, the phase separation takes place, and the concentrated phase grows in two kinetic mechanisms: The nucleation-and-growth (in the meta-stable region) and spinodal decomposition (in the spinodal region).[27-30] In the former mechanism, after the formation of concentrated phase nuclei, the nuclei grow according to the Ostwald ripening.[31] Because the equilibrium concentration of small concentrated-phase droplets is higher than that of large droplets, the small droplets were dissolved into metastable solutions, and large droplet grows by redepositing the dissolved solute component in the Ostwald ripening process. Lifshitz and Slyosov[32] formulated the size distribution function of the droplet in the late stage of the Ostwald ripening. The droplets grow continuously with the number-average radius being proportional to the one third power of the time, and m_w/m_n to be 1.15. In the spinodal decomposition, the bicontinuous network structure with the characteristic wavelength develops in the phase separating solution.

I-3. Phase Separation in the Aqueous Solution of Poly(*N*-isopropylacrylamide)

Poly(*N*-isopropylacrylamide) (PNIPAM) is a well-known thermoresponsive polymer, and the phase behavior of its aqueous solution has been extensively studied both experimentally and theoretically for many years.[33-36] It can be simply synthesized via free-radical polymerization from *N*-isopropylacrylamide monomer that is commercially available. At room temperature, PNIPAM is miscible in water, and after the temperature reaches ca. 30 °C or higher, the phase separation takes place in the aqueous solution. Based on this phase separation behavior, researchers are interested in potential applications of this polymer and its gel to tissue engineering and drug deliver[37-40] as the phase separation temperature of PNIPAM is near the temperature of human body.

Figure I-3 shows the chemical structure and pictures of the aqueous solution in the one-phase and two-phase regions. While the solution is transparent in the one-phase region, it transforms to “milky” solution. This milky solution however does not lead to macroscopic phase separation, even when it keeps standing for a long time (more than 1 day). This indicates that the concentrated-phase droplets formed in the solution stop growing at some stage. Thus, the Ostwald ripening does not occur in the phase-separating aqueous PNIPAM solution, being different from normal phase-separating polymer solutions.

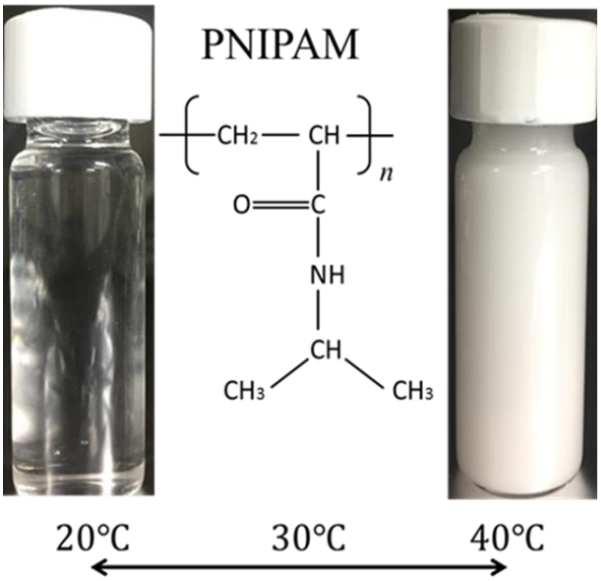

Figure I-3. Chemical structure of PNIPAM and appearance of its aqueous solution (c = 0.01 g/cm^3) in the one-phase (at 20 °C) and two-phase (at 40 °C) regions.

Figure I-4 displays the phase diagram of the aqueous PNIPAM solution obtained by Afroze *et al*.[40] using turbidity and differential scanning calorimetry. The binodal curve is very flat, remarkably different from normal phase-separating polymer solutions. Furthermore, the phase diagram of the aqueous PNIPAM - sensitively depend not only on the molecular weight of PNIPAM, but also on the chain-end groups, stereoregularity, randomly branched structure, and so on.[35] Those dependences are so complex that its phase diagram is still unpredictable, despite

of the long research history of PNIPAM for more than 50 years. [35]

In addition to the above complexity, Kawaguchi et al. [42] pointed out that the transmittance of light through the aqueous PNIPAM solution did not approach to 0 even at a temperature higher than the cloud-point temperature, so that the macroscopic phase separation does not take place in the solution at the cloud point and then the cloud-point curve does not necessarily correspond to the binodal. This finding asks questions about previously reported phase diagrams.

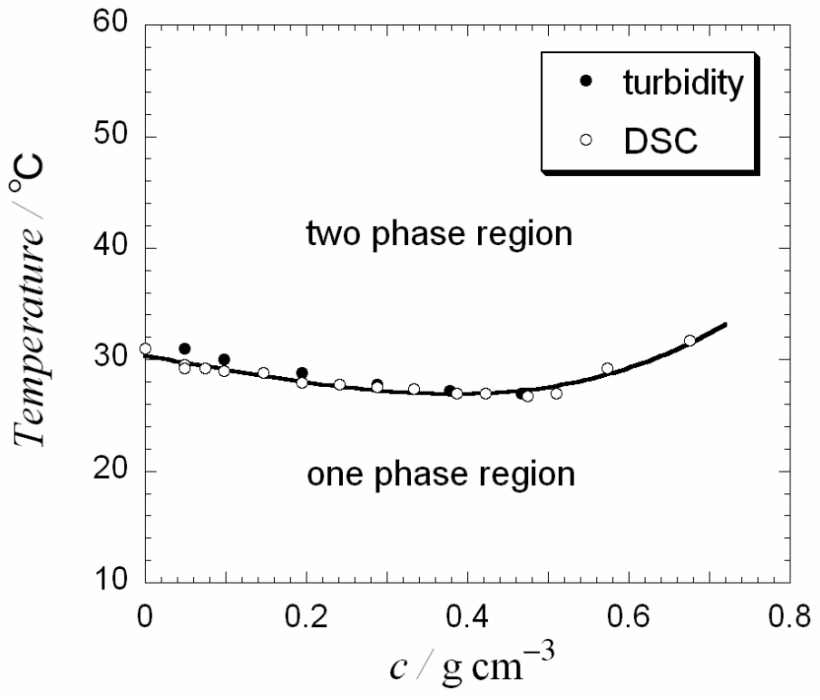

Figure 1-4. Phase diagram of the aqueous PNIPAM solution obtained by Afroze et al.[40] using turbidity and differential scanning calorimetry.

I-4. Thermosensitive Block Copolymers in Solution

When drugs and chemicals are incorporated into and released from nano-carriers and nano-reactors, it is convenient that amphiphilic block copolymers can form and collapse the micelle upon heating and cooling. For this reason, polymer scientists are recently very much interested in thermosensitive block copolymers as "smart materials." So far, many

thermosensitive block copolymers have been synthesized and their self-association behavior was investigated.[43-51]

However, as pointed out by Sato and Takahashi,[43] if the temperature change does not lead to strong enough amphiphilicity to the block copolymer, the copolymer cannot form the micelle but undergoes the liquid-liquid phase separation to form spherical droplets of the concentrated phase. They examined the competition between the micellization and liquid-liquid phase separation using the lattice model theory, and obtained the phase diagram as shown in Figure I-5.[43] When the interaction parameter χ_{AS} between the block chain A and solvent is constant, and the interaction parameter χ_{BS} between the block chain B and solvent increases, i.e., the amphiphilicity of the block copolymer increases, the solution first existing in the one phase region goes into the two phase region of the liquid-liquid phase separation, and then into the micellization region, where the micelle coexists with the copolymer single chain. Some thermosensitive block copolymers were reported to undergo the liquid-liquid phase separation upon heating.[49-51]

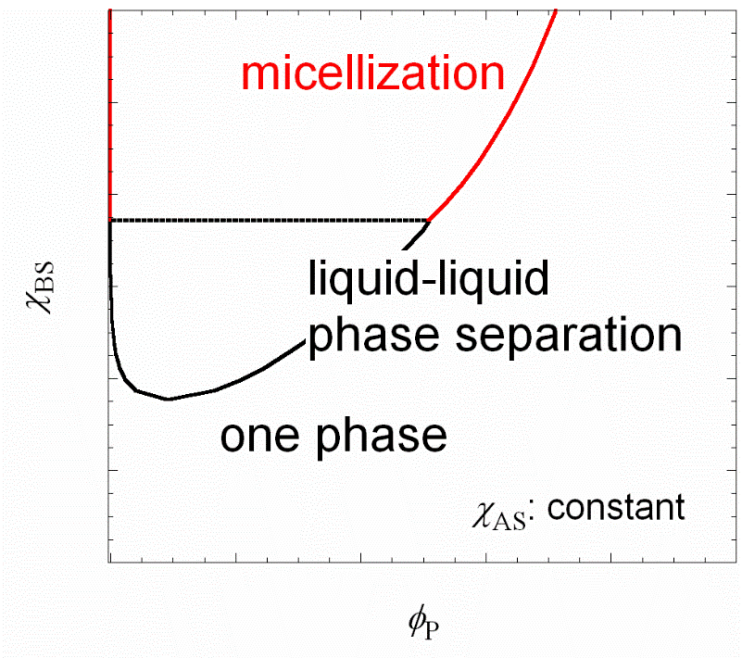

Figure I-5. Phase diagram for the amphiphilic block copolymer solution, where the liquid-liquid phase separation and micellization are competing.[43] Here, the abscissa is the copolymer volume fraction in the solution, and the coordinate is the interaction parameter χ_{BS} between the block chain B and solvent. The interaction parameter χ_{AS} between the block chain A and solvent keeps constant.

I-5. Scope of This Research

This dissertation deals with the competition between micellization and liquid-liquid phase separation in thermosensitive block copolymer solutions, using poly(*N*-isopropylacrylamide)-*b*-poly(*N*-vinyl-2-pyrrolidone) (PNIPAM-*b*-PNVP; cf Chart I-1) as the thermosensitive block copolymer. As mentioned above, PNIPAM becomes hydrophobic above ca. 30 °C, while PNVP is hydrophilic even at high temperatures close to the boiling temperature of water. Thus, the interaction parameter between PNIPAM and water (χ_{BS} in Figure I-5) can be changed by temperature to examine the competition between micellization and liquid-liquid phase separation.

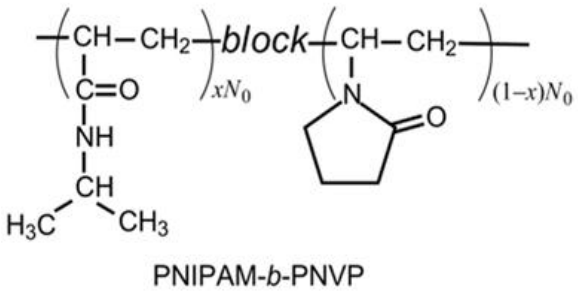

PNIPAM-*b*-PNVP

Chart I-1. Chemical structure of poly(*N*-isopropylacrylamide)-*b*-poly(*N*-vinyl-2-pyrrolidone) (PNIPAM-*b*-PNVP), where N_0 is the degree of polymerization of whole block copolymer, x is the ratio of PNIPAM chain

Prior to study the competition between micellization and liquid-liquid phase separation in aqueous solutions of PNIPAM-*b*-PNVP, Chapter II describes small angle X-ray scattering (SAXS) investigations of the dispersion state in a phase separating aqueous PNIPAM homopolymer solution at different temperatures. As mentioned in Section I-3, the phase-separating aqueous PNIPAM does not obey the Ostwald ripening but keeps the colloidal state. To my best knowledge, the dispersion state in the phase separating aqueous PNIPAM has not been studied by SAXS so far, although the globule state of the PNIPAM chain was investigated in very dilute solution by light scattering.[52]

In Chapter III, the competition between the micellization and liquid-liquid phase separation is studied both theoretically and experimentally. Using the lattice model theory of Sato and Takahashi,[43] I have investigated the composition and molecular weight dependences of the block copolymer on the competition. To compare these theoretical results, I have studied the dispersion state in aqueous solutions of PNIPAM-*b*-PNVP with different PNIPAM contents and molecular weights upon heating by SAXS.

Chapter IV describes the study on the dispersion state in aqueous solutions of mixtures of PNIPAM-*b*-PNVP block copolymer and the PNIPAM homopolymer upon heating, expecting that

the competition between the micellization and liquid-liquid phase separation can be controlled by addition of the PNIPAM homopolymer to the block copolymer solution. The dispersion state of each polymer component may be also affected by the existence of another polymer component. In fact, a macroscopic phase separation was observed in the mixture solution, though not observed in the individual polymer solutions.

Chapter V summarizes the results and conclusions obtained in this dissertation.

References

1. Turner, C. E.; Burridge, K. *Curr. Opin. Cell Biol.* **1991**, *3*, 849-853.
2. Aaron, J.; Travis, K.; Harrison, N.; Sokolov, K. *Nano Lett*. **2009,** *9*, 3612-3618.
3. Danino, D. *Curr. Opin. Colloid Interface Sci.* **2012**, *17*, 316-329.
4. Kim, Y.; Cao, Z.; Tan, W. *Proc. Natl. Acad. Sci.* **2008**, *105*, 5664-5669.
5. Wang, H.; Yang, R.; Yang, L.; Tan, W. *ACS Nano* **2009**, *3*, 2451-2460.
6. Akiyoshi, K.; Sunamoto, J. *Supramol. Sci*. **1996**, *3*, 157-163.
7. Nomura, Y.; Ishii, Y.; Takahashi, K. *Biosci. Biotechnol. Biochem*. **2009**, *73*, 926-929.
8. Segré, D.; Ben-Eli, D.; Deamer, D.W.; Lancet, D. *Orig. Life Evol. Biosph*. **2001**, *31*, 119-145.
9. He, Q.; Cui, Y.; Li, J. *Chem. Soc. Rev*. **2009**, *38*, 2292-2303.
10. Kono, K.; Murakami, E.; Hiranaka, Y.; Yuba, E.; Kojima, C.; Harada, A; Sakurai, K. *Angew. Chem*. **2011**, *50*, 6332-6336.
11. Makino, A.; Kizaka-Kondoh, S.; Yamahara, R.; Hara, I.; Kanzaki, T.; Ozeki, E.; Hiraoka, M.; Kimura, S. *Biomaterials* **2009**, *30*, 5156-5160.
12. Makino, A.; Kimura, S. *React. Funct. Polym*. **2011**, *71*, 272-279.
13. Vriezema, D. M.; Comellas Aragonès, M.; Elemans, J. A.; Cornelissen, J. J.; Rowan, A. E.; Nolte, R.J . *Chem. Rev*. **2005**, *105*, 1445-1490.
14. Vriezema, D. M.; Garcia, P. M.; Sancho Oltra, N.; Hatzakis, N. S.; Kuiper, S. M.; Nolte, R. J.; Rowan, A. E.; van Hest, J. C. *Angew. Chem. Int. Ed*. **2007**, *46*, 7378-7382.
15. Maiti, S.; Fortunati, I.; Ferrante, C.; Scrimin, P.; Prins, L.J. *Nat. Chem*. **2016**, *8*, 725-731.
16. Adams, M. L.; Lavasanifar, A.; Kwon, G. S. *J. Pharm. Sci*. **2003**, *92*, 1343-1355.

17. Alexandridis, P.; Lindman, B. 2000. *Amphiphilic block copolymers: self-assembly and applications*. Elsevier, 2000.
18. Sumi, T.; Sekino, H. *J. Chem. Phy.* **2005***, 122*, 194910-194921.
19. Budkov, Y. A.; Vyalov, I. I.; Kolesnikov, A. L.; Georgi, N.; Chuev, G. N.; Kiselev, M. G. *J. Chem. Phys*. **2014**, *141*, 204904-204912.
20. Parviz, B. A.; Ryan, D.; Whitesides, G. M. *IEEE Trans. Adv. Packag.***2003**, *26*, 233-241.
21. Malenfant, P. R.; Wan, J.; Taylor, S. T.; Manoharan, M. *Nat. Nanotechnol*. **2007**, *2*, 43-6.
22. Black, C.T. *ACS Nano* **2007**, *1*, 147-150.
23. Charleux, B.; Delaittre, G.; Rieger, J.; D'Agosto, F. *Macromolecules* **2012**, *45*, 6753-6765.
24. Matsumura, Y.; Maeda, H. *Cancer Res*. **1986**, *46*, 6387-6392.
25. Israelachvili, J. N. *Intermolecular and Surface Forces* (3rd Ed.), Elsevier, 2011.
26. Flory, P. J. *Principles of Polymer Chemistry*, Cornell University Press, 1953.
27. Gunton, J. D.; San Miguel, M.; Sahni, P. S. in *Phase Transition and Critical Phenomena*, edited by C. Domb and J. L. Lebowitz, Academic Press, 1983, Vol. 8, Chapt. 3 .
28. Kuwahara, N.; Kubota, K. *Phys. Rev. A* **1992**, *45*, 7385-7394.
29. Nunes, S. P.; Inoue, T. *J. Membr. Sci*. **1996**, *111*, 93-103.
30. Kim, K. Y.; Kang, S. L.; Kwak, H. Y. *Polym. Eng. Sci*. **2004**, *44*, 1890-1899.
31. Madras, G.; McCoy, B. J. *Chem.Eng.Sci*. **2002**, 57, 3809-3818.
32. Voorhees, P. W. *Annu. Rev. Mater. Sci*. **1992**, *22*, 197-215.
33. Heskins,; M. Guillet, J. E. *J. Macromol. Sci. Part A* **1968**, *2*, 1441–1455.
34. Plunkett, K. N.; Zhu, X.; Moore, J. S.; Leckband, D. E. *Langmuir* **2006**, *22*, 4259-4266.
35. Halperin, A.; Kroeger, M.; Winnik, F. M. *Angew. Chem. Int. Ed*. **2015**, *54*, 15342-15367.
36. Haq, M. A.; Su, Y.; Wang, D. *Mater. Sci. Eng.* **2017**, *70*, 842-855.
37. von Recum, HA.; Kikuchi, A.; Okuhara, M.; Sakurai, Y.; Okano, T.; Kim, SW. *J Biomater. Sci. Polym. Ed*. **1998**, *9*, 1241–1253.
38. Chung, J. E.; Yokoyama, M.; Yamato, M.; Aoyagi, T.; Sakurai, Y.; Okano, T. *J. Control. Release*. **1999**, *62*, 115–127.
39. Yan, H.; Tsujii, K. *Colloids Surf B*. **2005**, *46*, 142-146.
40. Lee, Elaine L.; Horst A. Von Recum. *J. Biomed. Mater. Res. A*. **2010**, *93* 411-418.
41. Afroze, F.; Nies, E.; Berghmans, H. *J. Mol. Struct*. **2000**, *554*, 55-68.

42. Kawaguchi, T.; Kojima, Y.; Osa, M.; Yoshizaki, T. *Polym. J*. **2008**, *40*, 455-459.
43. Sato, T.; Takahashi, R. *Polym. J*. **2017**, *49*, 273-277.
44. Zhu, P. W.; Napper, D. H. *Langmuir* **2000**, *16*, 8543-8545.
45. Zhang, W.; Shi, L.; Wu, K.; An, Y. *Macromolecules* **2005**, *38*, 5743-5747.
46. Kjøniksen, A.L.; Zhu, K.; Pamies, R.; Nyström, B. *J. Phys. Chem. B*. **2008**, *112*, 3294-3299.
47. Mori, H.; Ebina, Y.; Kambara, R.; Nakabayashi, K. *Polym. J*. **2012**, *44*, 550-560.
48. Ma, X.; Usui, R.; Kitazawa, Y.; Kokubo, H.; Watanabe, M. *Polym. J*. **2015**, *78*, 42-50.
49. Takahashi, R.; Sato, T.; Terao, K.; Qiu, X.-P.; Winnik, F. M. *Macromolecules* **2012**, *45*, 6111−6119.
50. Sato, T.; Tanaka, K.; Toyokura, A.; Mori, R.; Takahashi, R.; Terao, K.; Yusa, S. *Macromolecules* **2013**, *46*, 226−235.
51. Takahashi, R.; Qiu, X.-P.; Xue, N.; Sato, T.; Terao, K.; Winnik, F. M. *Macromolecules* **2014**, *47*, 6900−6910.
52. Wu, C.; Wang, X. *Phys. Rev. Lett.* **1998,** *80,* 4092−4094.

Chapter II

Phase Separation in Aqueous Solutions of Thermosensitive Polymer Poly(*N*-isopropylacrylamide) upon Heating.

II-1. Introduction

Ever since it was demonstrated that an aqueous solution of poly(*N*-isopropylacrylamide) (PNIPAM) underwent phase separation upon heating,[1,2] much attention has been paid for the phase separation behavior and its application such as drug delivery system and tissue engennering.[3,4] At the application of this polymer to various purposes, the phase diagram is the most fundamental property of its aqueous solution, and PNIPAM is one of the polymers of which phase behavior has been studied most extensively so far, as reviewed by Halperin et al. [5]

The cloud point curves[6,7] and calorimetric transition point curves[7,8] of aqueous solutions of PNIPAM were reported over a wide range concentration by many reserachers. However, those curves were very flat or had broad minima at very high concentrations (~ 40−50 wt%). Moreover, those curves reported often shifted towards the higher temperature side with increasing the molecular weight. These phase diagrams for the aqueous PNIPAM are quite anomalous when compared with phase diagrams of typical polymer-poor solvent systems and with the Flory-Huggins theory.[9] The theory predicts that the critical volume ϕ_c fraction of polymer and critical interaction parameter χ_c are related to the relative chain length P by[9]

$$\phi_c = P^{-1/2}, \quad \chi_c = \frac{1}{2} + P^{-1/2} \tag{II-1}$$

According to the equations, the minimum of the binodal curve must be located at considerably low polymer concentrations for high polymers, and the critical point for higher P must not be

located in the biphasic region for lower *P*. Many phase diagrams of aqueous PNIPAM solutions reported so far disagreed with these predictions.

However, it was pointed out by Kawaguchi et al.[10] that the phase separation of aqueous solution of PNIPAM should not be treated as general phase separation of polymer solutions. In the first place, the cloud points and binodal points are not identical in a solution of a polymer bearing molecular weight dispersity. Therefore, the direct measurements of the concentration of the concentrated and dilute phases would be necessary.

In general, binodal curves are made by measuring the concentrations of dilute-phase and concentrated-phase under macroscopically phase-separated conditions, however that procedure is difficult for aqueous solutions of PNIPAM. The reason is that the concentrated droplet phase stops growing to form colloidal particles of the hydrodynamic radius of a few hundred nm.[11−15] This phenomenon is responsible for high surface viscosity of concentrated droplet phase[16−18] and electrostatic repulsion,[19] and such droplet is often called as *mesoglobule*. In the extreme case of the high molecular weight and the low concentration of PNIPAM in water, the single chain coil−globule transition was reported by Wu *et al.*[20]

(Meso)globules may be considered as the concentrated (or polymer-rich) phase kinetically-trapped, and we refer to it as the *concentrated phase droplet* here. In fact, Balu et al.[19] have reported that an aqueous solution of PNIPAM exhibits macroscopic phase separation by adding LiCl. In addition, Takahashi et al.[18] have demonstrated that in an aqueous solution of PNIPMA-*b*-poly(2-isopropyl-2-oxazoline), whether macroscopic phase separation takes place or not can be controlled by adding methanol and changing temperature to adjust the interfacial viscosity and the interfacial solvophilicity of the concentrated droplet phase.

In the present study, I investigate the dispersion state in aqueous PNIPAM solutions over

a wide temperature range covering one-phase and two-phase regions by small-angle X-ray scattering (SAXS) measurements. The SAXS results are compared with the above-mentioned previous results of the phase separation behavior of aqueous PNIPAM.

II-2. Experimental Section

II-2-1. Polymer Samples and Solutions Preparation.

A PNIPAM sample were purchased from Polysciences, Inc., Pennsylvania, USA. According to the supplier, the PNIPAM sample was synthesized via free radical polymerization in dioxane using 2,2'-azobisisobutyronitrile as an initiator. The sample was fractionated using acetone and hexane as solvent and precipitant, respectively, on the basis of the literature.[21] The fraction used in this study has the weight-average molecular weight $M_{w,1}$, the dispersity index $M_{w,1}/M_{n,1}$, and the second virial coefficient $A_{2,1}$ (in 25 and 29 °C water) listed in Table II-1. The fraction of raceme diads of the sample was 0.5 ± 0.02, determined by ^{1}H NMR according to Ref 22.

Table II-1. Molecular Characteristics of the PNIPAM Fraction Used.

Fraction	$M_{w,1}$/g mol^{-1} [a]	$A_{2,1}$ [a,b]	$M_{w,1}/M_{n,1}$ [c]
PNIPAM-120k	12.4×10^4	3.4 (25 °C), 2.6 (29 °C)	1.09

[a]Determined by static light scattering. [b]In units of 10^{-4}cm^{3}g^{-2}mol. [c]Determined by SEC.

The PNIPAM fraction was dissolved in water deionized using a Millipore Milli-Q system to use for SAXS measurements. The polymer weight fraction w of the test solution was fixed to be 2 %, and the polymer mass concentrations c at different temperatures were calculated from w multiplied by the water density at each temperature.

II-2-2. SAXS measurements.

Synchrotron radiation SAXS measurements were carried out at the BL40B2 beamline, SPring-8, Hyogo. The wavelength of the incident light and the camera distance were fixed to be 0.1 nm and 4 m, respectively. A single quartz cell (the inner diameter: 2.0 mm) with a rubber cap was used in all measurements. Temperature of the cell holder was controlled by a thermostat HCS302 (Instec, Inc., Colorado). Since the capillary cell was thin enough, the temperature of the test solution was regarded to be identical with the temperature of cell holder, elevating the temperature with a heating rate of 1 °C/min from 25 to 73 °C. The scattering intensity of each solution was accumulated for 2 min by using a Dectris PILATUS2M instrument and circularly averaged. The polymers were not damaged by the X-ray irradiation, and the solvent was not vaporized by heating, checked by measuring the solution at 25 °C again at last.

The scattering intensity was calibrated so as to agree the excess SAXS Rayleigh ratio $R_{\theta,\mathrm{X}}$ with the light-scattering excess Rayleigh ratio for the aqueous PNIPAM solution at 25 °C. The SAXS optical constant K_e was calculated by[24]

$$K_\mathrm{e} = N_\mathrm{A} {a_\mathrm{e}}^2 \left(\frac{n_{\mathrm{e},0}}{M_0} - \frac{\bar{\upsilon} n_\mathrm{solv}}{\bar{\upsilon}_\mathrm{solv} M_\mathrm{solv}} \right)^2 \tag{II-2}$$

Here, N_A is the Avogadro constant, a_e is the classical electron radius, $n_{\mathrm{e},0}$ ($n_{\mathrm{e,solv}}$) and M_0 (M_solv) are the electron number and the molar mass of the monomer unit (the solvent), respectively, and $\bar{\upsilon}$ and $\bar{\upsilon}_\mathrm{solv}$ are the polymer partial specific volume and solvent specific volume, respectively.

II-3. Results

Figure II-1 shows SAXS scattering functions as the double-logarithmic plots of $R_{\theta,\mathrm{X}}/K_\mathrm{e}c$ vs k for the 2 wt% aqueous solution of the fraction PNIPAM-120 k at 25 – 35 °C. Here, $R_{\theta,\mathrm{X}}$ is

the excess SAXS Rayleigh ratio at the scattering angel θ, K_e is the SAXS optical constant calculated by eq II-2, c is the polymer mass concentration, and k is the magnitude of the scattering vector. In the low k region ($k < 0.1$ nm^{-1}), the scattering intensity increases with increasing temperature, indicating the formation of large scattering components with increasing temperature. On the other hand, at $k > 0.2$ nm^{-1}, the scattering intensity keeps constant at 25, 29, 31, and 33 °C, but abruptly decreases at 35 °C. The scattering in the high k region mainly arises from the PNIPAM single chains molecularly dispersed in the aqueous solution. The data points at 0.3 nm^{-1} < k < 2 nm^{-1} almost obey the line with a slope slightly large than –2, expected for the Gaussian chain. The single chain component were not practically observed at 35 °C.

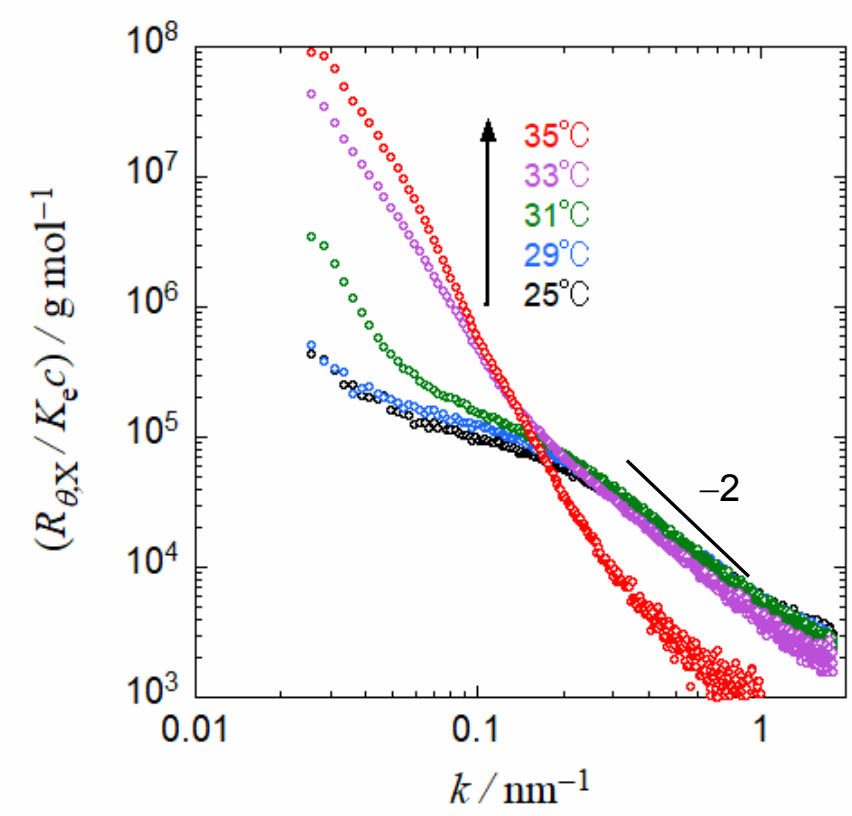

Figure II-1. SAXS profiles of the aqueous solution of the fraction PNIPAM-120k (w = 0.02) at 25, 29, 31, 33, and 35 °C. The segment indicates the slope of k^{-2}.

Figure II-2 shows SAXS scattering profiles for the aqueous PNIPAM solution at 25, 35, 57, and 73 °C. Above 35 °C, the scattering function does not essentially change with temperature, although we can observe a little bit shifts downward with increasing temperature from 35 °C. The scattering intensity at 35 °C and higher almost obey a line with the slope of –4 in an intermediate k range (0.1 $nm^{-1} < k < 0.3$ nm^{-1}). This slope implies that the large scattering component at the high temperatures is polydisperse spheres. Although the scattering intensity is weak, the data points at high temperatures slightly deviate upward from the line with the slope –4 at $k > 0.3$ nm^{-1}. This may come from a tiny amount of PNIPAM single chains or their small aggregates remaining even at the high temperatures.

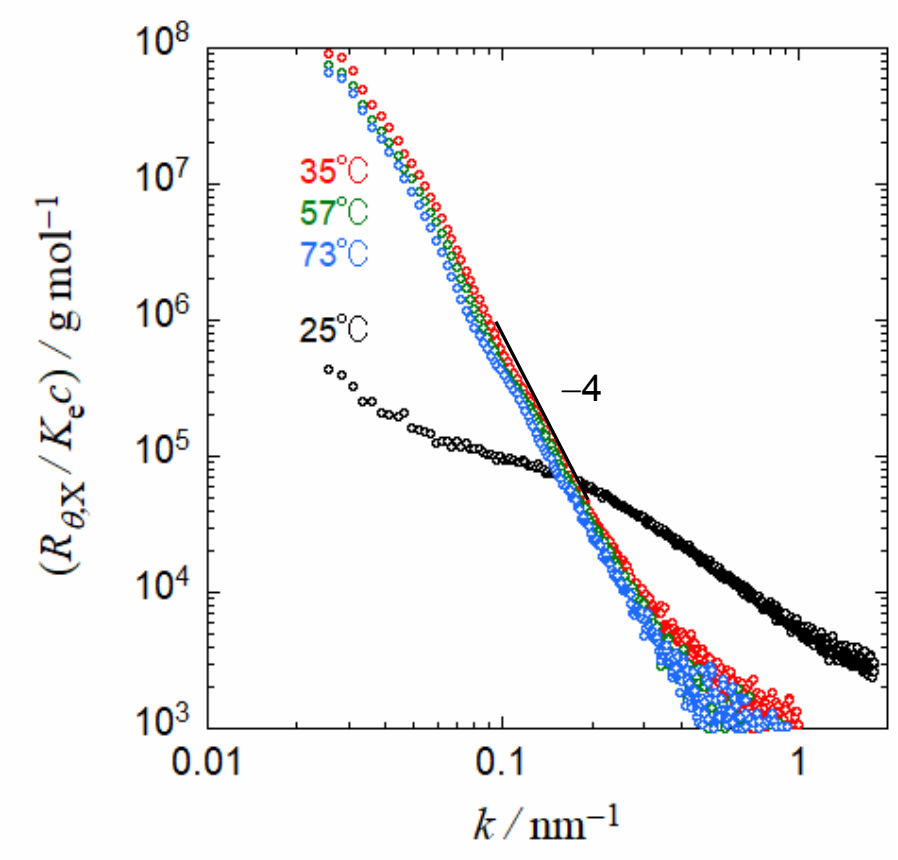

Figure II-2. SAXS profiles of the aqueous solution of the fraction PNIPAM-120k (w = 0.02) at 25, 35, 57, and 73 °C. The segment indicates the slope of k^{-4}.

II.4. Discussion

As shown in Figures II-1 and II-2, the SAXS scattering function for the aqueous PNIPAM solution is remarkably different below and above 35 °C. In the following, we analyze the SAXS scattering function separately below and above 35 °C.

II-4-1. Analysis of the Scattering Function below 35 °C.

At 25 °C, water is a good solvent for PNIPAM, because the second virial coefficient $A_{2,1}$ is positive (cf. Table II.1), and PNIPAM may exist as a flexible chain affected by the intramolecular excluded volume effect in 25 °C water. Yoshizaki and Yamakawa[25] calculated the particle scattering function $P(k)$ for the unperturbed wormlike chain, and proposed an empirical function to represent the calculation results as a function of k as well as the persistence length q and the Kuhn statistical number N (or the contour length L) of the wormlike chain, given by

$$P(k) = \left[\left(1 - \mathrm{e}^{-\xi^{-5}}\right) P_{(\mathrm{C}^*)}(k; R_\mathrm{g}) + \mathrm{e}^{-\xi^{-5}} P_{(\mathrm{R})}(k; L)\right] \Gamma(k; N, \xi) \exp\left(-\tfrac{1}{16} d^2 k^2\right) \qquad \text{(II-3)}$$

where R_g is the radius of gyration of the chain (calculated from q and N), ξ is defined by

$$\xi \equiv \left(\frac{\pi}{2N}\right)\left(\frac{R_\mathrm{g}}{2q}\right)^2 (2qk) \qquad \text{(II-4)}$$

and $P_{(\mathrm{C}^*)}(k; R_\mathrm{g})$ and $P_{(\mathrm{R})}(k; L)$ are the known particle scattering functions for the Gaussian coil with the same R_g as that of the wormlike chain, and the rod with the contour length L. Numerical results for $P(k)$ cannot be expressed by an average of $P_{(\mathrm{C}^*)}(k; R_\mathrm{g})$ and $P_{(\mathrm{R})}(k; L)$ in the bracket of eq II-3, so that we need the correction factor $\Gamma(k; N, \xi)$ in eq II-3 which is a function of k, N, and ξ, formulated by the original authors. The last exponential function in eq II-3 is the correction factor of the finite thickness of the polymer chain, where d is the polymer chain thickness.

Pedersen and Schurtenberger[26] made off-lattice Monte Carlo simulations on the discrete

wormlike chain with the excluded volume interaction to calculate the perturbed particle scattering function $P(k)$. Calculated results for the perturbed $P(k)$ are expressed in a similar form to eq II-3 for the unperturbed one. While the particle scattering function of the rod $P_{(\mathrm{R})}(k; L)$ is not affected by the excluded volume interaction, that of the Gaussian coil $P_{(\mathrm{C}^*)}(k; R_\mathrm{g})$ is perturbed by the interaction. Furthermore, the parameter ξ is replaced by

$$\xi' \equiv \left(\frac{\pi}{1.103N}\right)^{3/2} \left(\frac{R_\mathrm{g}}{2q}\right)^{2.564} (2qk) \tag{II-5}$$

and numerical coefficients in the correction function $\Gamma(k; N, \xi)$ are dependent on the perturbation. The perturbed particle scattering function is given by

$$P(k) = \left[\left(1 - \mathrm{e}^{-\xi'/5}\right) P'_{(\mathrm{C}^*)}(k; R_\mathrm{g}) + \mathrm{e}^{-\xi'/5} P_{(\mathrm{R})}(k; L)\right] \Gamma'(k; N, \xi') \exp\left(-\tfrac{1}{16} d^2 k^2\right) \tag{II-6}$$

with the perturbed functions $P'_{(\mathrm{C}^*)}(k; R_\mathrm{g})$ and $\Gamma'(k; N, \xi)$ given by the original authors.

At a finite polymer concentration, the scattering function is affected by the inter-molecular interference, and it may be written in the form[27]

$$\frac{R_{\theta,\mathrm{X}}}{K_\mathrm{e} c} = \frac{M_{\mathrm{w},1} P(k)}{1 + 2M_{\mathrm{w},1} P(k) A_{2,1} c} \tag{II-7}$$

where $M_{\mathrm{w},1}$ and $A_{2,1}$ are the weight-average molar mass and the second virial coefficient, respectively, for the polymer. The particle scattering function $P(k)$ is calculated by eq II-3 or II-6.

Figure II-3 displays the Kratky plot for the aqueous PNIPAM solution at 25, 29, 31, and 33 °C shown in Figure II-1. According to the Debye function[28] for the Gaussian chain, the Kratky plot reaches to a plateau in a high k region, but the experimental Kratky plots keep increasing with increasing k. This may come from the chain connectivity and radial distribution of the excess electron density of the PNIPAM chain. Equations II-3 and II-6 include these effects on the scattering function. In Figure II-3, red solid, black solid, and black dotted curves indicate

theoretical values calculated by eq II-7 along with $P(k)$ calculated by eqs II-6, II-3, and $P_{(C^*)}(k; R_g)\exp(-d^2k^2/16)$, respectively. At 25 and 29 °C, $A_{2,1}$ is positive, and the intra-molecular excluded volume effect may be important. Thus, the red solid curves show the best fitting with the experimental data. At 31 and 33 °C, dehydration takes place on the PNIPAM chain, and water becomes a poor solvent, although no light-scattering $A_{2,1}$ has not reported. The experimental Kratky plot can be fitted by the black solid curves for the unperturbed wormlike chain.

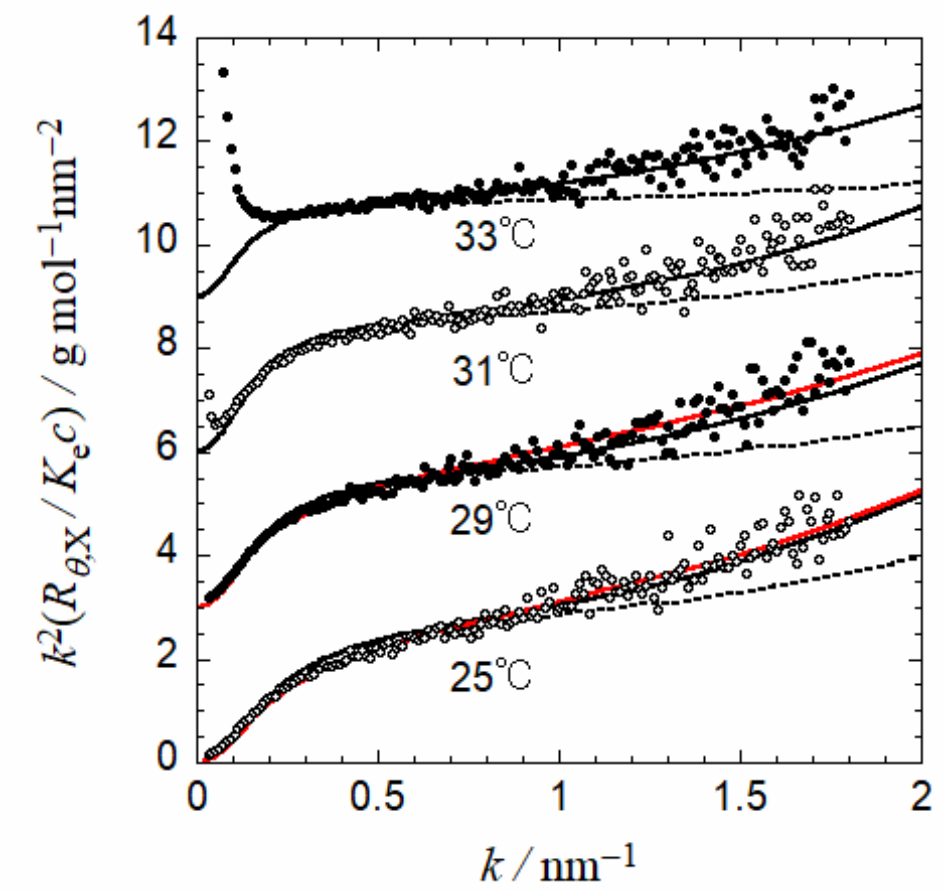

Figure II-3. Kratky plots for the aqueous PNIPAM solution at 25, 29, 31, and 33 °C shown in Figure II-1. Red solid, black solid, and black dotted curves, $P_1(k)$ calculated by eqs II-6, II-3, and $P_{(C^*)}(k; R_g)\exp(-d^2k^2/16)$, respectively. Plots for 29, 31, and 33 °C shift upward for viewing clarity.

Table II-2 lists fitting parameters used to calculate the Kratky plots in Figure II-3. Values of $M_{w,1}$ and $A_{2,1}$ at 25 and 29 °C consistent with light scattering results shown in Table II-1, and the perturbed R_g is slightly larger than unperturbed $R_{g,0}$. The q values indicate that the PNIPAM is a flexible polymer, but it turns out that the chain stiffness effect is important at high k from the comparison between the black solid and dotted curves at each temperature. The intra-molecular attractive interaction may be important in the PNIPAM chain at 33 °C, however there are no theoretical calculations of such attractive interaction effect on $P(k)$. Although the experimental Kratky plot seems to be fitted by the black solid curve, the fitting parameter values may be affected by this attractive interaction. Thus, we do not argue the values of $A_{2,1}$ and q at 33 °C. At last, d^2 values in the rightmost column in Table II-2 are negative, which are physically unreasonable. However, as pointed out by Arakawa, et al. [29] inhomogeneous radial distribution of the excess electron density of the polymer chain can give negative d^2 values, if the correction factor $\exp(-d^2k^2/16)$ is used in eqs II-3 and II-6. The radial electron density distribution of the hydrated PNIPAM chain may be responsible for the negative d^2.

Table II-2. Fitting parameters for the single chain used in the Kratky plots at 25, 29, 31, and 33 °C.

Temp	$M_{w,1}$[a]	$A_{2,1}$[b]	q/nm	L/nm (N[c])	$R_{g,0}$/nm[d]	R_g/nm	d^2/nm^2
25 °C	12.4	3.0	1.0	280 (140)	9.6	10	–0.1
29 °C	12.4	1.6	1.0_5	280 (130)	9.8	10	–0.08
31 °C	12.4	0.8	1.0_5	280 (130)	9.8	–	–0.08
33 °C	12.4	0	1.5	280 (93)	12	–	–0.05

[a] In units of 10^4 g/mol. [b] In units of 10^{-4} cm^{3}g^{-2}mol. [c] Calculated by $L/2q$. [d] Unperturbed radius of gyration calculated from q and N.

Although the scattering function in the low k region is not inconspicuous in the Kratky plot in Figure II-3, upswings in the low k region are definitely observed even at 25 and 29 °C in Figure II-1. These upswings indicate the existence of large scattering components. As listed in Tables II-1 and II-2, the second virial coefficient $A_{2,1}$ is positive at 25 and 29 °C, so that water is a good solvent for PNIPAM at those temperatures. However, it has been sometimes reported the formation of large polymer aggregates even in good solvents.[30-33] Combining static and dynamic light scattering, Kawaguchi *et al*.[10] demonstrated that PNIPAM form large aggregates in water even at temperatures considerably lower than the cloud point, and the aggregating component may be loosely packed random coils, judged from the ratio ρ of the radius of gyration to the hydrodynamic radius.

We express the loosely packed random coils by randomly cross-linked Gaussian chains, illustrated in Figure II-4. The z-average particle scattering function $P_{\mathrm{agg,z}}(k)$ for the randomly cross-linked Gaussian chain may be represented by[34]

$$P_{\mathrm{agg,z}}(k) = \frac{1-\dfrac{\alpha}{1+\alpha}\left(1-\dfrac{\sin bk}{bk}\right)}{1+\dfrac{(f-1)\alpha}{1-(f-1)\alpha}\left(1-\dfrac{\sin bk}{bk}\right)} P_{(\mathrm{C}^*)}\left(k; b/\sqrt{6}\right) \qquad \text{(II-8)}$$

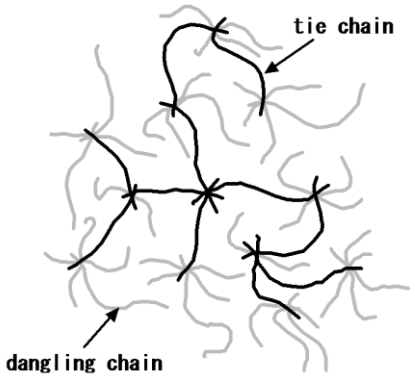

Figure II-4. Schematic diagram of a randomly cross-linked Gaussian chains as a model for the loosely packed random coil.

where f and α are the functionality and the reaction rate of the cross-link point, respectively, b is the average end-to-end distance of the tie chain connecting the nearest neighbor cross-link points, and $P_{(C^*)}(k;\ b/6^{1/2})$ is the Debye function for the Gaussian chain with the radius of gyration of $b/6^{1/2}$. The weight-average number $m_{w,tie}$ of tie chains per aggregate is given by

$$m_{w,tie} = \frac{1+\alpha}{1-(f-1)\alpha} \tag{II-9}$$

which diverges at $\alpha = 1/(f-1)$.

Because the inter-molecular interference for the large scattering component (component 2) becomes sharply unimportant with increasing k, we consider the inter-molecular interference effect only among single chains (component 1). As a result, the scattering function can be written as[35]

$$\frac{R_{\theta,X}}{K_e c} = \frac{w_1 M_{w,1} P_1(k)}{1+2w_1 M_{w,1} P_1(k) A_{2,1} c} + w_2 M_{w,2} P_2(k) \tag{II-10}$$

where w_i, M_i, and $P_i(k)$ are the weight fraction in the total polymer, the weight-average molar mass, and (z-average) particle scattering function of component i (i = 1, 2), respectively, and $A_{2,1}$ is the second virial coefficient for component 1. Equation II-3 or II-6 is used for $P_1(k)$, and $P_{agg,z}(k)$ in eq II-8 for $P_2(k)$. The weight-average molar mass $M_{w,2}$ of component 2 is calculated by $m_{w,tie}$ (given by eq II-8) multiplied by the molar mass of the tie chain M_{tie} (of which average end-to-end distance is b).

Figure II-5 demonstrates that the SAXS scattering function for aqueous PNIPAM solution at 25 and 29 °C can be nicely fitted by eq II-10 along with eqs II-8 and II-9. The fitting parameters used for these fittings are listed in Table II-3. The weight fraction w_2 of the aggregating component is very tiny, and the aggregation number $m_{w,tie}$ is quite large, which are

characteristic to polymer aggregates in good solvents.

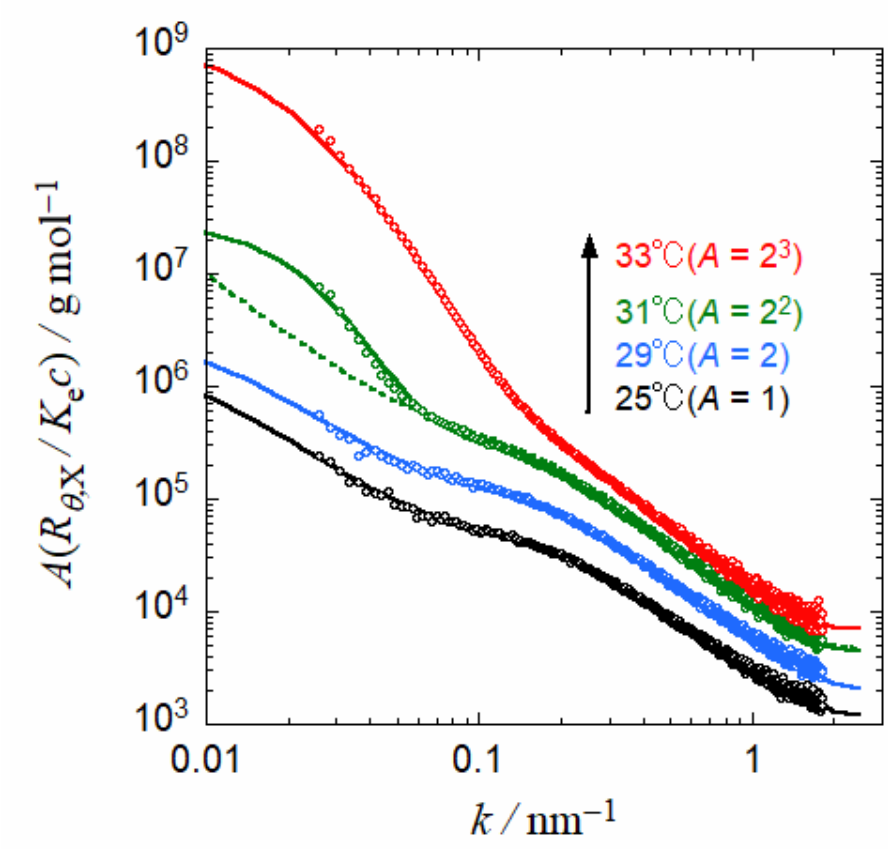

Figure II-5. Fitting results of the SAXS scattering function for aqueous PNIPAM solution at 25-33 °C.

Table II-3. Fitting parameters for the aggregating component at 25, 29, 31, and 33 °C.

Temp.	w_2	f [a]	α	$m_{w,tie}$	$R_{g,agg,z}$/nm	M_{tie} [b]	b/nm
25 °C	0.0055	4	0.3332	3,300	190	1.4	5.4
29 °C	0.008	4	0.3331	1,900	160	1.8	6.1
Temp.	w_2	$M_{w,2}$ [c]	$M_{w,2}$/ $M_{n,2}$	c_{in} [d]	$R_{g,agg,z}$/nm		
31 °C	0.02	5.0	4	0.22	100		
33 °C	0.35	5.6	22	0.18	180		

[a] Assumed to be 4. [b] In units of 10^4 g/mol. [c] In units of 10^8 g/mol. [d] In units of g/cm^3.

On the other hand, the same fitting by eq II-10 along with eqs II-8 and II-9 was impossible for the scattering functions at 31 and 33 °C in the low k region. Thus, the large scattering component at 31 and 33 °C is not loosely packed random coils of the PNIPAM chain. With increasing the temperature, the degree of dehydration of the PNIPAM chain increases to make the attractive interaction among PNIPAM chains stronger, and the aqueous PNIPAM solution may go into the biphasic region of the phase diagram. In the biphasic region, concentrated-phase droplets may be formed in the dilute aqueous PNIPAM solution. The concentrated-phase droplets are regarded as polydisperse spherical particles, of which z-average particle scattering function $P_{z,2}(k)$ can be expressed by[36]

$$P_{z,2}(k) = {M_{w,2}}^{-1} \int_0^\infty \left[3 \times \frac{\sin(kR) - kR\cos(kR)}{(kR)^3} \right]^2 M w_2(M) \mathrm{d}M \tag{II-11}$$

where R is the radius of the sphere with the molar mass M, calculated by

$$R = \left(\frac{3M}{4\pi N_A c_{in}} \right)^{1/3} \tag{II-12}$$

with the Avogadro constant N_A and the polymer mass concentration c_{in} inside the spherical particle. The molar mass distribution function (the weight fraction) $w_2(M)$ of the spherical particles in eq II-11 is assumed to obey a log-normal distribution:

$$w_2(M) = \frac{1}{\sqrt{2\pi \ln\left(M_{w,2}/M_{n,2}\right)} M} \exp\left[-\frac{\ln^2\left(M/\sqrt{M_{w,2}M_{n,2}}\right)}{2\ln\left(M_{w,2}/M_{n,2}\right)} \right] \tag{II-13}$$

with $M_{w,2}$ and $M_{n,2}$ being the weight-average and number-average molar mass of the polydisperse spherical particles.

Equation II-10 along with eq II-11 instead of eq II-8 can fit the scattering functions at 31 and 33 °C in the low k region (cf. solid curves in Figure II-5). The fitting parameters are listed in

Table II-3.

At present, we do not know the relation between the loose aggregation at 25 and 29 °C and the phase separation at 31 and 33 °C. As mentioned above, the loose aggregation takes place under the good solvent condition, indicating that it may have nothing to do with the attractive interaction inducing the phase separation. When the loose aggregation contributes to turbidity of the solution, the cloud point is not necessarily the indication of the start of the phase separation, as pointed out by Kawaguchi et al.[10]

II-4-2. Analysis of the Scattering Function at Temperatures ≥ 35 °C.

As indicated in Figure II-2, the scattering function in the high k region abruptly diminishes at temperatures ≥ 35 °C, demonstrating the disappearance of PNIPAM single chains in the aqueous solution. The phase separation makes the single chains to coagulate and to form the concentrated phase; the coexisting dilute phase has little single chain component. The k^{-4} decay of the scattering function at temperatures ≥ 35 °C demonstrates that the main scattering component is the polydisperse spherical particles, i.e., concentrated-phase droplets.

Taking into account the inter-particle interference effect among spherical particles, we write the scattering function in the following form[27]

$$\frac{R_\theta}{Kc} = \frac{M_{w,2} P_{z,2}(k)}{1 + 2M_{w,2} P_{z,2}(k) A_{2,2} c} \qquad \text{(II-14)}$$

where $A_{2,2}$ is the (average) second virial coefficient for spherical particles, and the z-average particle scattering function is calculated by eq II-11 with eqs II-12 and II-13. In Figure II-6, solid curves indicate theoretical values by using parameter values listed in Table II-4. The fitting parameters are very insensitive to the temperature. Only $M_{w,2}$ slightly increases with the temperature. It is interesting that c_{in} is not only insensitive to the temperature but also

considerably low. We will discuss this result in the next subsection.

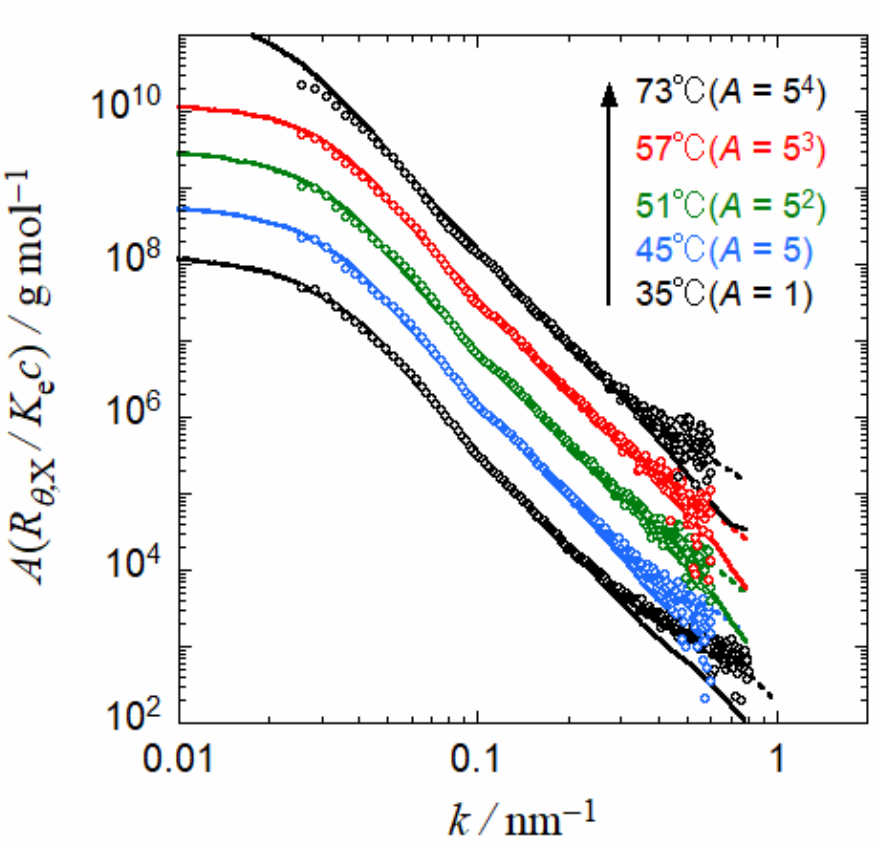

Figure II-6. Fitting results of the SAXS scattering function for aqueous PNIPAM solution at temperatures ≥ 35 °C.

Table II-4. Fitting parameters for concentrated-phase droplets at temperatures ≥ 35 °C.

Temp	$M_{w,2}$ [a]	$M_{w,2}/M_{n,2}$	c_{in} [b]	$R_{g,agg,z}$/nm	$A_{2,2}$ [c]
35 °C	2.8_5	4	0.18	$97._5$	1.0
45 °C	3.8	4	0.18	110	1.5
51 °C	4.7_5	4	0.18	120	1.5
57 °C	4.7_5	4	0.18	120	2.0
73 °C	6.6_5	4	0.17_5	130	0.28

[a] In units of 10^8 g/mol. [b] In units of g/cm^3. [c] In units of 10^{-8} cm^{3}g^{-2}mol.

Although the high-k scattering intensity is weak, the data points at high temperatures slightly deviate upward from the line with the slope –4 at $k > 0.3$ nm^{-1}. This may come from a tiny amount of PNIPAM single chains or their small aggregates remaining even at the high temperatures. Considering this minor scattering component, we modify the scattering function from eq II-14 to

$$\frac{R_\theta}{Kc} = w_1 M_{w,1} P_1(k) + \frac{w_2 M_{w,2} P_{z,2}(k)}{1 + 2 M_{w,2} P_{z,2}(k) A_{2,2} c} \tag{II-15}$$

where w_1, $M_{w,1}$, and $P_1(k)$ are the weight fraction, the weight-average molar mass, and the particle scattering function of the minor small component, respectively. Here, this minor component is assumed to be a globule of the PNIPAM single chain, of which particle scattering function is given by that for the uniform density sphere:[36]

$$P_1(k) = \left[3 \times \frac{\sin(kR) - kR\cos(kR)}{(kR)^3} \right]^2 \tag{II-16}$$

where R is the radius of the globule. If there is not water inside the globule, the polymer concentration inside the globule should be identical with the reciprocal of the specific volume for PNIPAM (= 0.9 cm^3/g). Using eq II-12 with $M = 12.4 \times 10^4$ g/mol and $c_{in} = 1.1$ g/cm^3, R is estimated to be 3.5 nm.

Figure II-7 plots $k^4 R_{\theta,X}/K_e c$ against k for the temperatures ≥ 35 °C. Although data points are rather scattered, the upswing of the plot in the high k region at each temperature (especially at 35 °C) may indicate the existence of small globule component. Solid curves are obtained from eq II-15 with $M_{w,1} = 12.4 \times 10^4$ g/mol and $R = 3.5$ nm. Values of w_1 chosen are shown in the right side of Figure II-7. When the solid curve is compared with the dashed curve obtained with $w_1 = 0$ at each temperature, the first term in the right-hand side of eq II-15 appreciably contributes to the

scattering function at high k.

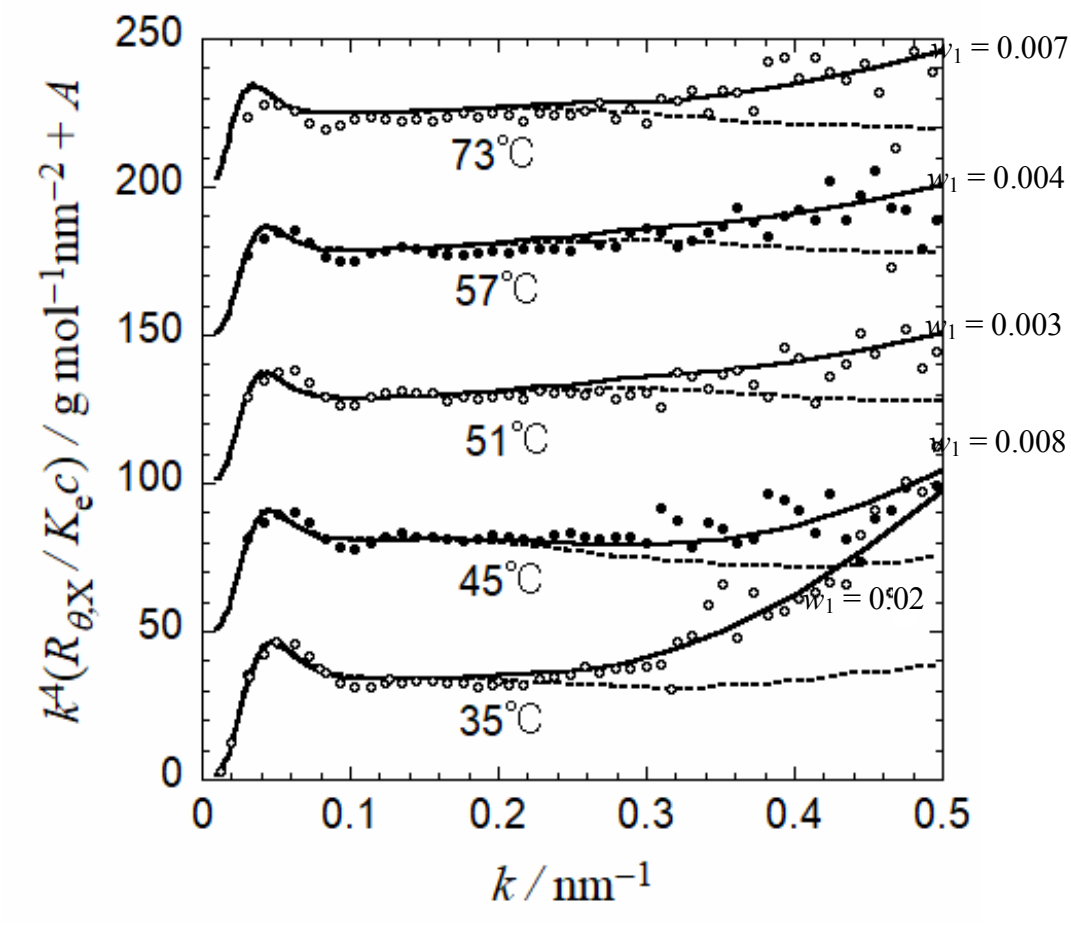

Figure II-7. Fitting results of the SAXS scattering function for aqueous PNIPAM solution at temperatures ≥ 35 °C. Solid and dashed curves, theoretical values calculated by eq II-15 and eq II-14 ($w_1 = 0$ in eq II-15), respectively.

II-4-3. Phase diagram.

Afroze et al.[6] carried out turbidity and DSC measurements on aqueous PNIPAM solution over a wide range of the polymer concentration, where the molecular weight of the PNIPAM sample is 12×10^4 being quite close to our PNIPAM sample. Figure II-8 shows their experimental results of the cloud point temperature (unfilled black circles) and the temperature at

the beginning of the endotherm (filled black circles). Although the former temperature is slightly higher than the latter temperature at $c < 0.3$ g/cm^3, both data points form a composite curve. However, as pointed out by Kawaguchi et al.[10] and also mentioned above (cf. Figure II-5 and Table II-3), the random aggregation first occurs among PNIPAM chains in water upon heating. This random aggregation may contribute to turbidity and endotherm of the aqueous PNIPAM solution, but it may not directly relate to the phase separation. Thus, the solid curve connecting black circles may not be the binodal curve.

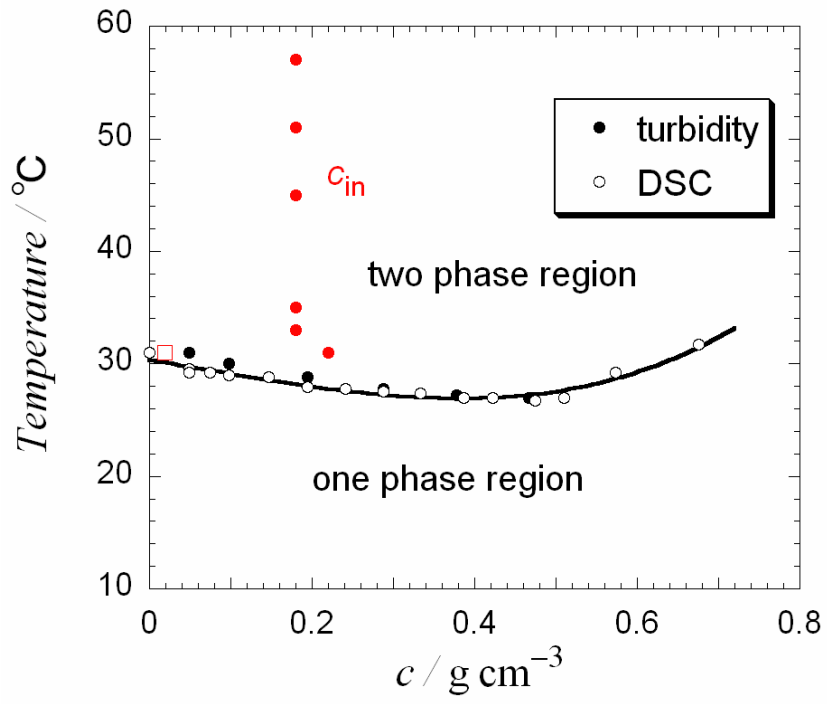

Figure II-8. Polymer mass concentrations c_{in} inside the spherical particles obtained by SAXS (red filled circles) and the temperature where the SAXS profile starts showing the k^{-4} dependence in the low k region (red square), plotted in the phase diagram to compare the results obtained by Afroze et al.[6]

The SAXS profile of the aqueous PNIPAM solution (c = 0.02 g/cm^3) abruptly diminishes in the high k region at 35 °C (cf. Figure II-1), indicating that PNIPAM single chains disappear in the solution to form polydisperse spherical particles. Thus, we can say that the red square in the phase diagram of Figure II-8 is inside the biphasic region. Furthermore, the upswing of the SAXS profile in the low k region (cf. Figure II-5) becomes steep at 31 and 33 °C, and can be fitted not by the loosely packed random coil or the randomly cross-linked Gaussian chain but by polydisperse spherical particle model. This indicates that the binodal temperature at c = 0.02 g/cm^3 is as low as 31 °C (the square in Figure II-8), which is close to the cloud point temperature and the temperature at the beginning of the endotherm obtained by Afroze et al.[6]

SAXS profiles for the phase separating aqueous PNIPAM solution at temperatures ≥ 35 °C provide polymer mass concentrations c_{in} inside the spherical particles. The results of c_{in} are plotted by red filled circles in the phase diagram of Figure II-8. Those red circles are inside the two-phase region, and remarkably deviate from the solid curve obtained by turbidity and DSC measurements. This demonstrates that spherical particles in the phase-separating aqueous solution are not pure coexisting concentrated phase, but include coexisting dilute phase. Not only c_{in} but also the SAXS profile itself do not essentially change with temperature above 35 °C. Therefore, the dispersion state in the phase-separating PNIPAM solution may be frozen above 35 °C. The dehydration upon heating makes PNIPAM so hydrophobic that inter- and intra-molecular attractive interaction may exceed thermal energy to prohibit the molecular chain rearrangement above 35 °C. Therefore, the dispersion state in the phase-separating PNIPAM solution above 35 °C may not be the thermodynamically equilibrium state. This makes the study of aqueous PNIPAM solution difficult.

II-5. Conclusions

The phase separation behavior of the aqueous PNIPAM solution upon heating was investigated by SAXS, and the following conclusions were obtained:

(1) Below 35 °C, the main component in the solution is the single random coil chain, of which SAXS scattering function is fitted by flexible wormlike chains with or without the excluded volume effect.

(2) At 25 and 29 °C, the solution contains a minor scattering component of the loosely packed random coil viewed as the randomly cross-linked Gaussian chain.

(3) At 31 and 33 °C, the minor component changes from the loosely packed random coil to polydisperse spherical particles. This is the indication of the phase separation

(4) At and above 35 °C, the main component in the solution changes from the single random coil chain to the spherical particle. However, the SAXS profile does not essentially alter with temperature above 35 °C. This indicates that the phase-separating PNIPAM solution above 35 °C is not the thermodynamically equilibrium state. The polymer concentration inside the spherical particle was much lower than the expected coexisting concentrated phase concentration.

(5) A tiny amount of small particles remains in the phase-separating solution above 35 °C. However, it is premature that this small particle component is the globule of the PNIPAM chain coexisting with the concentrated phase, because the solution is not in the thermodynamically equilibrium state.

References

1. Scarpa, J. S.; Mueller, D. D.; Klotz, I. M. *J. Am. Chem. Soc.* **1967,** *89,* 6024−6030.
2. Heskins, M.; Guillet, J. E. *Sci. Chem.* **1968,** *A2,* 1441−1455.
3. Schild, H. G. *Prog. Polym. Sci.* **1992,** *17,* 163−249.

4. Aseyev, V.; Tenhu, H.; Winnik, F. M. *Polym. Sci.* **2011,** *242,* 29−89.
5. Halperin, A.; Kroger, M.; Winnik, F. M. *Angew. Chem. Int. Ed.* **2015,** *127,* 15558−15586.
6. Afroze, F.; Nies, E.; Berghmans, H. *J. Mol. Struct.* **2000,** *554,* 55−68.
7. Zhou, X.; Li, J.; Wu, C.; Zheng, B. *Rapid Commun.* **2008,** *29,* 1363−1367.
8. Durme, K. V.; Assche, G. V.; Mele, B. V. *Macromolecules* **2004,** *37*, 9596−9605.
9. Flory, P. J. *Principle Polymer Chemistry*, Cornell Univ. Press, Ithaca, New York, 1953.
10. Kawaguchi, T.; Kobayashi, K.; Osa, M.; Yoshizaki, T. *J. Phys. Chem. B* **2009,** *113,* 5440−5447.
11. Ding, Y.; Ye, X.; Zhang, G. *J. Phys. Chem. B* **2008,** *112*, 8496−8498.
12. Gorelov, A. V.; Chesne, A. D. *Physica A* **1997,** *240,* 443−452.
13. Dawson, K. A.; Gorelov, A. V.; Timoshenko, E. G.; Kuznetsov, Y. A.; Chesne, A. D. *Physica A.* **1997,** *244,* 68−80.
14. Aseyev, V.; Tenhu, H.; Winnik, F. M. *Adv. Polym. Sci.* **2006,** *196,* 1−85.
15. Aseyev. V.; Hietala, S.; Laukkanen, A.; Nuopponen, M.; Confortini, O; Prez, F. E. D.; Tenhu, H. *Polymer.* **2005,** *46,* 7118−7131.
16. Tanaka, H. *Macromolecules* **1992,** *25,* 6377−6380.
17. Zhang, G.; Wu, C. *Adv. Polym. Sci.* **2006,** *195,* 101−176.
18. Takahashi, R.; Qiu, X.-P.; Xue, N.; Sato, T.; Terao, K.; Winnik, F. M. *Macromolecules.* **2014,** *47,* 6900−6910.
19. Balu, C.; Delsanti, M.; Guenoun, P. *Langmuir* **2007,** *23,* 2404−2407.
20. Wu, C.; Wang, X. *Phys. Rev. Lett.* **1998,** *80,* 4092−4094.
21. Fujishige, S. *Polym. J.* **1987,** *19,* 297−300.
22. Kobayashi, K.; Yamada, S.; Nagaoka, K.; Kawaguchi, T.; Osa, M.; Yoshizaki, T. *Polym J.* **2009,** *41,* 416−424.
23. Kujawa, P.; Winnik, F. M. *Macromolecules* **2001,** *34,* 4130–4135.
24. Takahashi, R.; Sato, T.; Terao, K.; Yusa, S.. *Macromoleues.* **2015,** *48,* 7222−7229.
25. Yamakawa, H.; Yoshizaki, T. *Helical wormlike chains in polymer solutions* (Vol. 1). Berlin: Springer, **1997**.
26. Pedersen, J.S.; Schurtenberger, P. *Macromolecules***1996**, *29*, 7602-7612.
27. Sato, T.; Jinbo, Y.; Teramoto, A. *Polym. J.* **1999,** *31,* 285−292.
28. Debye, P. *J. Phys. Colloid Chem.* **1947,** *51,* 18−32.

29. Arakawa, S.; Terao, K.; Kitamura, S.; Sato, T. *Polym. Chem*, **2012**, *3*, 472-478.
30. Guenet, J. M., NFF, W.; PA, E. *Polym. Commun*. **1983**, *24*, 230
31. Koberstein, J.T., Picot, C. and Benoit, H. *Polymer* **1985**, *26*, 673-681.
32. Gan, J.Y., Francois, J. and Guenet, J.M. *Macromolecules* **1986**, *19*, 173-178.
33. Kanao, M.; Matsuda, Y.; Sato, T. *Macromolecules* **2003,** *36,* 2093−2102.
34. Kajiwara. K; Burchard, W.; Gordon. M. *Br. Polym. J.* **1970**, *2*,110
35. Sato, T.; Tanaka, K.; Toyokura, A.; Mori, R.; Takahashi, R.; Terao, K.; Yusa, S. *Macromolecules* **2013,** *46,* 226−235.
36. Takahashi, R.; Sato, T.; Terao, K.; Qiu, X.-P.; Winnik, F. M. *Macromolecules* **2012,** *45,* 6111−6119.

Chapter III

Micellization and Phase Separation in Aqueous Solutions of Thermosensitive Block Copolymer Poly(*N*-isopropylacrylamide)-*b*-poly(*N*-vinyl-2-pyrrolidone) upon Heating.

III-1. Introduction

Strongly amphiphilic diblock copolymers consisting of polar and nonpolar block chains [*e.g.*, polystyrene-*b*-poly(acrylic acid) and polystyrene-*b*-poly(ethylene oxide)] are known to form different types of micelles in aqueous media.[1–6] These polymer micelles are much more stable with lower critical micelle concentrations than micelles of low-molar-mass surfactants. This stability is the merit of applications as nanocarriers and nanoreactors.

On the other hand, when the amphiphilicity of the diblock copolymer is not strong enough, the liquid–liquid phase separation is preferred to the micellization as the solvent becomes poor. If colloidal droplets of the concentrated phase in the phase-separating solution are stabilized by the more hydrophilic block chain covering the colloidal droplet surface, it is rather difficult to distinguish the spherical droplet of the concentrated phase from the spherical micelle. However, it is important to clarify the condition of the micellization and phase separation, because the spherical micelle has a definite hydrophobic core and a constant size, which is more useful to apply as nanocarriers and nanoreactors than the colloidal droplet of the concentrated phase.

Recently, many thermosensitive block copolymers have been synthesized and their self-assembly behavior in aqueous solution has been investigated,[7–15] because their micelles can

easily incorporate and release drugs and chemicals. However, these thermosensitive block copolymers often underwent liquid−liquid phase separations rather than the micellization, because of their weak amphiphilicity. In a previous study, Sato et al.[14] investigated the self-association of a thermosensitive block copolymer consisting of poly(*N*-isopropylacrylamide) and poly(*N*-vinyl-2-pyrrolidone) (PNIPAM-*b*-PNVP; cf. Scheme 1) in water upon heating by small-angle X-ray scattering (SAXS) and concluded that the phase separation rather than the micellization takes place in this copolymer solution, due to the weak amphiphilicity of the copolymer. Similar conclusions were obtained also for aqueous solutions of poly(2-isopropyl-2-oxazoline)-*b*-poly(2-ethyl-2-oxazoline)[13] and poly(2-isopropyl-2-oxazoline)-*b*-poly(*N*-isopropylacrylamide). [15] Additionally, Sato and Takahashi[16] demonstrated theoretically that weakly amphiphilic block copolymers prefer thermodynamically the liquid−liquid phase separation to the micellization in solution.

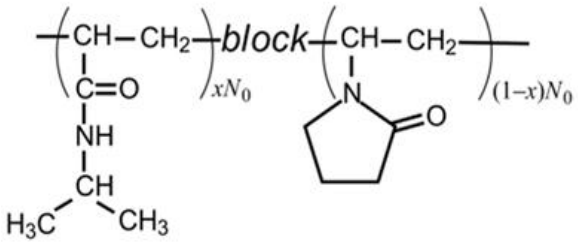

PNIPAM-*b*-PNVP

Scheme III-1. Chemical structure of poly(*N*-isopropylacrylamide)-*b*-poly(*N*-vinyl-2-pyrrolidone) (PNIPAM-*b*-PNVP)

When the block copolymer is used as nanocarriers or nanoreactors in solution, it is important to understand detailed conditions of the micellization and phase separation. In this study, we carried out SAXS measurements on aqueous PNIPAM-*b*-PNVP solutions to examine the competition between the micellization and phase separation by changing the degrees of

polymerization of both block chains. The experimental results were compared with the theory based on the lattice model.[14]

III-2. Theoretical Section

First, we briefly reviewed the previous lattice theory for block copolymer solutions.[14] According to the Flory-Huggins theory,[17] the mixing Gibbs energy per lattice site Δg_h of the homogeneous solution of the AB diblock copolymer, of which A and B block copolymer chains consist of P_A and P_B lattice units, respectively, is given by

$$\frac{\Delta g_h}{k_B T} = \phi_S \ln \phi_S + \frac{\phi_P}{P} \ln \phi_P + \bar{\chi} \phi_S \phi_P \qquad \text{(III-1)}$$

where $k_B T$ is the Boltzmann constant multiplied by the absolute temperature, ϕ_S and ϕ_P are the volume fractions of the solvent and copolymer, respectively, in the solution ($\phi_S = 1 - \phi_P$), P is the number of the total lattice units consisting of one copolymer chain (= $P_A + P_B$), x_A and x_B are the mole fractions of the A and B units in the copolymer chain ($x_A = P_A/P$, $x_B = P_B/P = 1 - x_A$), and $\bar{\chi}$ is the average interaction parameter between the block copolymer chain and solvent, defined by[18]

$$\bar{\chi} \equiv x_A \chi_{AS} + x_B \chi_{BS} - x_A x_B \chi_{AB} \qquad \text{(III-2)}$$

with χ_{AS}, χ_{BS}, and χ_{AB} being the interaction parameters between the A unit and solvent, between the B unit and solvent, and between the A and B units, respectively.

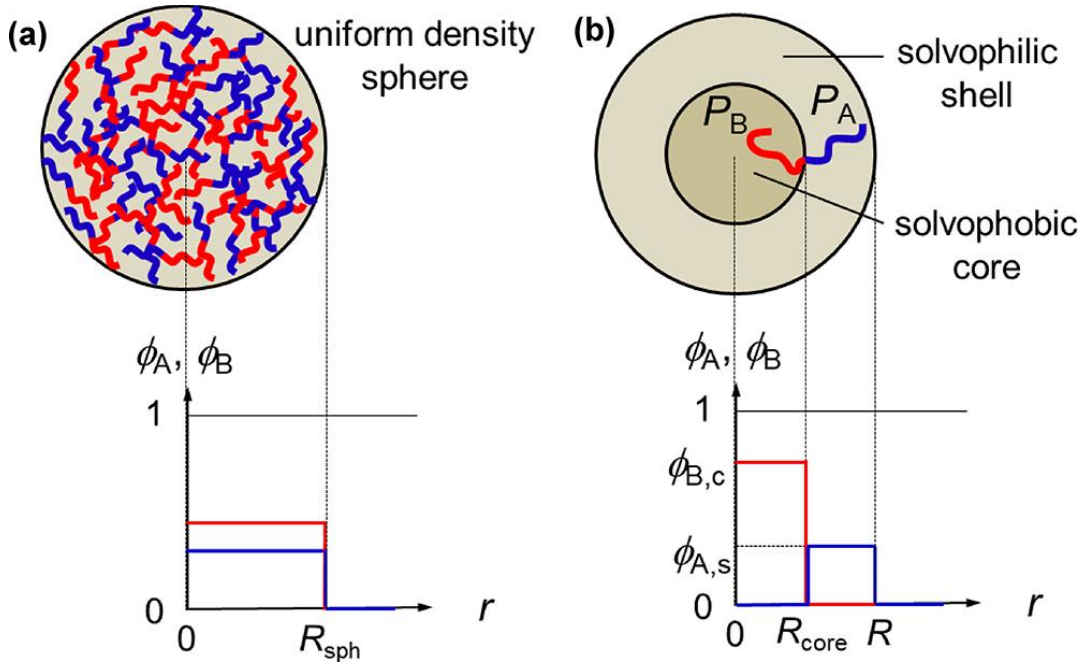

Figure III-1. Uniform density spherical droplet model (a) and a simplified model of the spherical micelle (b).

On the other hand, when the block copolymer forms a micelle in the solution illustrated in Figure III-1, the mixing Gibbs energy per lattice site Δg_m of the micellar phase is given by[16]

$$\frac{\Delta g_m}{k_B T} =$$

$$= \frac{\phi_P}{P}\left(\ln\kappa + \ln\phi_P\right) + \frac{R^3 - {R_{core}}^3}{R^3}\left(1-\phi_{A,s}\right)\ln\left(1-\phi_{A,s}\right) + \frac{{R_{core}}^3}{R^3}\left(1-\phi_{B,c}\right)\ln\left(1-\phi_{B,c}\right) \quad \text{(III-3)}$$

$$+\left[x_A\left(1-\phi_{A,s}\right)\chi_{AS} + x_B\left(1-\phi_{B,c}\right)\chi_{BS} - x_A x_B \chi_{AB}\right]\phi_P + \frac{3a{R_{core}}^2}{R^3}\frac{a^2\gamma}{k_B T}$$

with

$$\kappa = \frac{\pi}{27} P^{2+\alpha} x_A {x_B}^{1-2\alpha}\left({x_A}^{\alpha} + {x_B}^{\alpha}\right)^3 \quad \text{(III-4)}$$

Here, ϕ_P is the average copolymer volume fraction in the micellar phase and R and R_{core} are radii of the micelle and of the micellar core (cf. Figure III-1b), respectively, simply calculated by

$$R_{\mathrm{core}}/a = (x_{\mathrm{B}}P)^{\alpha}, \quad (R - R_{\mathrm{core}})/a = (x_{\mathrm{A}}P)^{\alpha} \tag{III-5}$$

with the unit lattice size a and an exponent α. In what follows, α is assumed to be 0.5 for the Gaussian chain. (Although α for the A and B block chains should be larger and smaller than 0.5, respectively, due to the excluded volume effect, final phase diagrams are almost independent ofthe values of α.) In the last term in eq III-3, γ is the interfacial tension between the core and shell regions. The volume fractions of the A block chain in the shell region $\phi_{\mathrm{A,s}}$ and of the B block chain in the core region $\phi_{\mathrm{B,c}}$ (cf. Figure III-1b) are given by

$$\phi_{\mathrm{A,s}} = \frac{R^3 x_{\mathrm{A}} \phi_{\mathrm{P}}}{R^3 - {R_{\mathrm{core}}}^3} = \frac{x_{\mathrm{A}} \left({x_{\mathrm{A}}}^{\alpha} + {x_{\mathrm{B}}}^{\alpha} \right)^3}{\left({x_{\mathrm{A}}}^{\alpha} + {x_{\mathrm{B}}}^{\alpha} \right)^3 - {x_{\mathrm{B}}}^{3\alpha}} \phi_{\mathrm{P}}, \quad \phi_{\mathrm{B,c}} = \frac{R^3 x_{\mathrm{B}} \phi_{\mathrm{P}}}{{R_{\mathrm{core}}}^3} = \frac{\left({x_{\mathrm{A}}}^{\alpha} + {x_{\mathrm{B}}}^{\alpha} \right)^3}{{x_{\mathrm{B}}}^{3\alpha - 1}} \phi_{\mathrm{P}} \tag{III-6}$$

The last interfacial energy term in eq III-3 can be calculated by[18]

$$\frac{a^2}{k_{\mathrm{B}}T}\gamma = \sqrt{\frac{1}{3}\left(\phi_{\mathrm{A,s}} + \phi_{\mathrm{B,c}}\right)\left\{ f\left(\tfrac{1}{2}\phi_{\mathrm{A,s}}, \tfrac{1}{2}\phi_{\mathrm{B,c}}\right) - \frac{1}{2}\left[f\left(\phi_{\mathrm{A,s}}, 0\right) + f\left(0, \phi_{\mathrm{B,c}}\right)\right]\right\}} \tag{III-7}$$

with the function $f(x, y)$ defined by

$$f(x,y) \equiv \left[\ln(1-x-y) + \chi_{\mathrm{AS}}x + \chi_{\mathrm{BS}}y\right](1-x-y) + \chi_{\mathrm{AB}}xy \tag{III-8}$$

Thus, when P, x_{B}, and α as well as χ_{AS}, χ_{BS}, and χ_{AB} are given, we can calculate Δg_{m} as a function of ϕ_{P} from the above equations III-3–III-8.

When χ_{AB} and χ_{AS} are fixed to be 0 and 0.4, respectively (α = 0.5), the binodal curve for the liquid−liquid phase separation in the χ_{BS}−ϕ_{P} phase diagram can be drawn from the common tangent of the Δg_{h}−ϕ_{P} curve given by eqs III-1 and III-2.[16] The results for several sets of P and x_{B} are drawn by black dashed and solid curves in Figure III-2, where panels a−c show the x_{B} dependence at fixed P = 200 and panels d−f display the P dependence at fixed x_{B} = 0.3 of the liquid−liquid phase separation diagram. When χ_{BS} is an increasing function of the temperature,

the phase diagrams have the lower critical solution temperatures.

On the other hand, if the common tangent can be drawn to the $\Delta g_h - \phi_P$ curve and $\Delta g_m - \phi_P$ curve (given by eqs III-3−III-8), the phase equilibrium between the dilute (or concentrated) copolymer phase and the micellar phase may be possible, and if the total Gibbs energy in this equilibrium state is lower than that at the liquid−liquid phase separation, the micellization prefers the liquid−liquid phase separation.[16] In the phase diagrams in Figure III-2, red solid curves (red dash-dot curves) are binodal curves for the dilute phase-micellar phase equilibrium (the concentrated phase-micellar phase equilibrium) which are thermodynamically more stable than the liquid−liquid phase separation. The black solid and dashed curves distinguish between thermodynamically stable and unstable binodal curves for the liquid−liquid phase separation.

As seen from panels a−c in Figure III-2, both binodal curves for the liquid−liquid phase separation and micellization go upward with decreasing x_B at fixed P, but the former shifts more rapidly, so that the micellization becomes more stable at lower x_B. On the other hand, panels d−f demonstrate that both binodal curves for the liquid−liquid phase separation and micellization go upward with decreasing P at fixed x_B, but the latter shifts more rapidly. Thus, the micellization becomes more stable at higher P. As χ_{BS} increases along the arrow in panels a, b, e, and f, the single-phase solution undergoes the liquid−liquid phase separation and then micellization. On the other hand, in panels c and d, the micellization takes place directly from the single-phase state with increasing χ_{BS}.

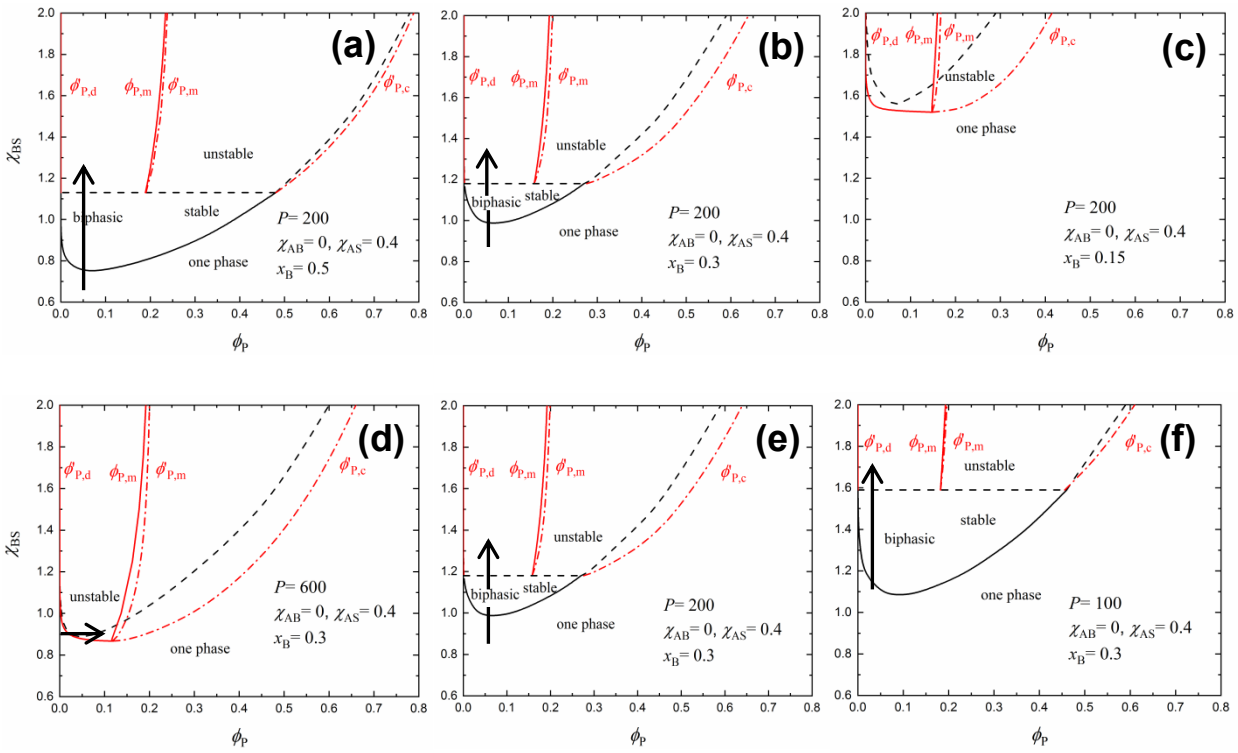

Figure III-2. Theoretical phase diagrams of block copolymer solutions with changing interaction parameter χ_{BS} at fixed χ_{AB} = 0 and χ_{AS} = 0.4. Panels a−c show the x_B dependence at fixed P = 200, and panels d−f display the P dependence at fixed x_B = 0.3 of the phase diagram. (Panels b and e are the same phase diagram.) The volume fractions of the coexisting dilute and micellar phases are denoted as $\phi'_{P,d}$ and $\phi_{P,m}$, respectively, and those of the coexisting concentrated and micellar phases as $\phi'_{P,c}$ and $\phi'_{P,m}$, respectively.

Strictly speaking, the micelle is not a thermodynamic phase but a thermodynamic component, which indicates that the micellization may not be regarded as the purely thermodynamic phase separation. As shown by the small arrow in panel d in Figure III-2, when ϕ_P increases at a fixed χ_{BS}, the single-phase solution transforms into the micellar solution at crossing the red solid curve. The concentration ϕ_P of the crossing point is referred to as the critical micelle concentration; however, it is not the phase transition point thermodynamically but a crossover point. Similarly, the phase boundary between the liquid−liquid phase separation

region and the micellization region in the phase diagrams of panels a, b, e, and f in Figure III-2 should also be regarded as a crossover between different self-association states of the block copolymer.

III-3. Experimental Section

III-3-1. Materials.

Ethyl-2-methyl-2-butyltelanilpropionate (BTEE) was gifted from Otsuka Chemical. *N*-Vinyl-2-pyrroridone (NVP) (99.9%) was gifted from Nippon Shokubai, which was distilled under reduced pressure. *N*-Isopropylacrylamide (NIPAM) (97%) from Sigma- Aldrich was recrystallized from a mixture of benzene and *n*-hexane (3/7, v/v). 2,2′-Azobis(isobutyronitrile) (AIBN, 98%) from Wako Pure Chemical was recrystallized from methanol. *N,N*-Dimethylformamide (DMF) was distilled under reduced pressure. Water was purified with a Millipore Milli-Q system. Other reagents were used as received.

III-3-2. Copolymer Samples.

Two PNIPAM-*b*-PNVP samples were used in this work. Both of them were synthesized according to the organotellurium-mediated controlled radical polymerization described in a previous paper.[10] The copolymer samples were purified by reprecipitating from chloroform into a large excess of diethyl ether twice. The polymers were dissolved in pure water and were recovered by a freeze-drying technique.

Molecular characteristics of these block copolymer samples are listed in Table III-1, along with those of the previously used sample. Number-average degrees of polymerization of the PNIPAM block chain $N_{0,n}$(PNIPAM) and of the PNVP block chain $N_{0,n}$(PNVP) as well as the

total number-average degree of polymerization $N_{0,n} = N_{0,n}(\text{PNIPAM}) + N_{0,n}(\text{PNVP})$ and the mole fraction of the NIPAM monomer unit in the copolymer chain $x = N_{0,n}(\text{PNIPAM})/N_{0,n}$ were determined by ^{1}H NMR. Dispersities in the molecular weight M_w/M_n of the copolymer samples were determined by size-exclusion chromatography (SEC) using polystyrene standard samples.[10]

III-3-3. Measurements.

^{1}H NMR spectra were obtained with a Bruker DRX-500 spectrometer. SEC measurements were performed using a Tosoh RI8021 refractive index detector equipped with two Shodex LF-804 polystyrene mixed gel columns at 40 °C under a flow rate of 0.5 mL/min. A DMF solution containing 10 mM LiBr was used as eluent. The obtained data were calibrated with standard polystyrene samples.

Table III-1. Molecular Characteristics of PNIPAM-*b*-PNVP Samples Used in This and Previous Studies

sample	$N_{0,n}$(PNIPAM) [a]	$N_{0,n}$(PNVP) [a]	$N_{0,n}$	x	M_w/M_n [b]	$M_w/10^4$ [c]
PNIPAM_{60}-*b*-PNVP_{368}	60	368	428	0.14	1.25	5.95
PNIPAM_{31}-*b*-PNVP_{120}	31	120	151	0.21	1.26	2.12
PNIPAM_{100}-*b*-PNVP_{218} [d]	100	218	318	0.31	1.16	4.12

[a]Determined by ^{1}H NMR. [b]Determined by SEC. [c]Weight-average molecular weights calculated by $[113N_{0,n}(\text{PNIPAM}) + 111N_{0,n}(\text{PNVP})]M_w/M_n$ using the results listed in the second, third, and sixth columns. [d]Sample used in the previous study.[14]

Small-angle X-ray scattering (SAXS) measurements of aqueous PNIPAM-*b*-PNVP solutions were performed on the BL40B2 beamline, SPring-8, Hyogo. The wavelength of the

incident light and the camera distance were fixed to be 0.1 nm and 4 m, respectively. For all measurements, a single quartz capillary cell (2.0 mm inner diameter) with a rubber cap was used. Since the capillary cell was thin enough, the temperature of each test solution was regarded to be identical with the temperature of cell holder, elevating the temperature with a heating rate of 1 °C/min from 20 to 75 °C. The scattering intensity of each solution was accumulated for 2 min by using a Dectris PILATUS2M instrument and circularly averaged.[19]

The SAXS excess Rayleigh ratio $R_{\theta,X}$ at the scattering angle θ and the optical constant K_e of SAXS were calculated by[20]

$$R_{\theta,\mathrm{X}} = F\left(\frac{I_{\theta,\mathrm{soln}}}{I_{\mathrm{mon,soln}}} - \frac{I_{\theta,\mathrm{solv}}}{I_{\mathrm{mon,solv}}}\right), \quad K_{\mathrm{e}} = N_{\mathrm{a}} {a_{\mathrm{e}}}^2 {\gamma_{\mathrm{av}}}^2 \tag{III-9}$$

Here, F is the instrument constant, $I_{\theta,\mathrm{soln}}$ ($I_{\theta,\mathrm{solv}}$) and $I_{\mathrm{mon,soln}}$ ($I_{\mathrm{mon,solv}}$) are the scattering intensity at the scattering angle θ and the incident SAXS intensity, respectively, of the solution (of the solvent), N_{a} is the Avogadro constant, a_{e} is the classical radius of an electron (=2.8 × 10^{-13} cm), and γ_{av} is the average SAXS contrast factor of the copolymer. The values of γ_{av} for the copolymer in water were calculated by

$$\gamma_{\mathrm{av}} = \frac{M_{0,\mathrm{NIPAM}} N_{0,\mathrm{n}}(\mathrm{PNIPAM}) \gamma_{\mathrm{PNIPAM}} + M_{0,\mathrm{NVP}} N_{0,\mathrm{n}}(\mathrm{PNVP}) \gamma_{\mathrm{PNVP}}}{M_{0,\mathrm{NIPAM}} N_{0,\mathrm{n}}(\mathrm{PNIPAM}) + M_{0,\mathrm{NVP}} N_{0,\mathrm{n}}(\mathrm{PNVP})} \tag{III-10}$$

with the contrast factors of the NIPAM and NVP monomer units given by

$$\gamma_{\mathrm{PNIPAM}} = \frac{n_{\mathrm{e,NIPAM}}}{M_{0,\mathrm{NIPAM}}} - \frac{\bar{\upsilon}_{\mathrm{PNIPAM}}}{\upsilon_{\mathrm{H_2O}}} \frac{n_{\mathrm{e,H_2O}}}{M_{\mathrm{H_2O}}}, \quad \gamma_{\mathrm{PNVP}} = \frac{n_{\mathrm{e,NVP}}}{M_{0,\mathrm{NVP}}} - \frac{\bar{\upsilon}_{\mathrm{PNVP}}}{\upsilon_{\mathrm{H_2O}}} \frac{n_{\mathrm{e,H_2O}}}{M_{0,\mathrm{H_2O}}} \tag{III-11}$$

where $n_{e,i}$ and $M_{0,i}$ (i = NIPAM, NVP, and H_2O) are the numbers of electrons and molar masses of the monomer units and water, respectively, $\bar{\upsilon}_{\mathrm{i}}$ is the partial specific volume of the monomer unit i (= PNIPAM and PNVP), and υ_{H2O} is the specific volume of water. By density measurements of the copolymer samples, the partial specific volumes were determined to be $\bar{\upsilon}_{\mathrm{PNIPAM}}$ = 0.863

cm^3/g and $\bar{\upsilon}_{PNVP}$ = 0.774 cm^3/g (γ_{PNIPAM} = 0.0692 mol/g; γ_{PNVP} = 0.1105 mol/g). Temperature dependences of γ_{PNIPAM} and γ_{PNVP} were neglected. The instrument constant F was determined so that the experimental scattering profile at 25 °C agrees with the theoretical one for the single chain (cf. eqs III-12−16 below).

Test solutions of 2.0 wt % for SAXS measurements were prepared by mixing the dried PNIPAM-*b*-PNVP sample and pure water and stirring the mixture at least overnight at room temperature.

III-4. Results and Discussions

III-4-1. SAXS Profiles.

Figure III-3 shows temperature dependences of SAXS scattering functions $R_{\theta,X}/K_e c$ for samples $PNIPAM_{60}$-*b*-$PNVP_{368}$ and $PNIPAM_{31}$-*b*-$PNVP_{120}$, where c is the copolymer mass concentration and k is the magnitude of the scattering vector. For both block copolymers, the intensity increases with the temperature at $k \lesssim 0.3$ nm $^{-1}$ but almost independent of the temperature at $k \gtrsim 0.3$ nm $^{-1}$. The increase in the scattering function in the low k region indicates the formation of a large scattering component upon heating, but the temperature insensitiveness of the scattering function in the high k region demonstrates that the original small scattering component at the room temperature exists even at high temperatures.

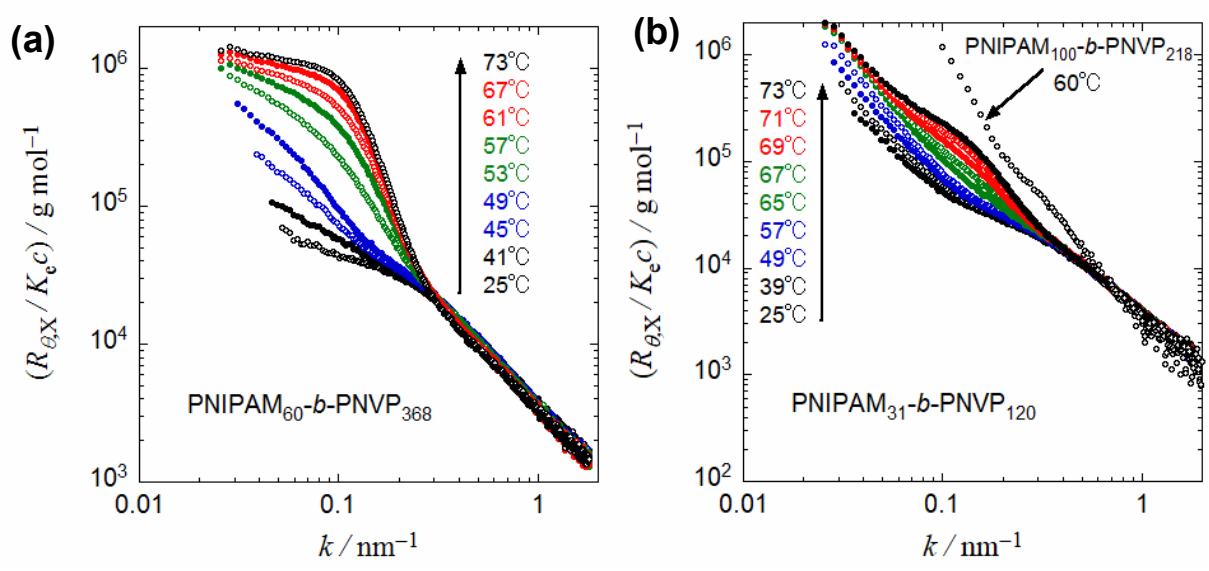

Figure III-3. SAXS profiles obtained for 2 wt% aqueous solutions of the block copolymer samples PNIPAM$_{60}$-*b*-PNVP$_{368}$ (a) and PNIPAM$_{31}$-*b*-PNVP$_{120}$ (b) upon heating from 25°C to 73°C with heating rate of 1°C/min. The SAXS scattering profile for 1 wt% aqueous solution of the sample PNIPAM$_{100}$-*b*-PNVP$_{218}$ at 60 °C obtained in the previous study[14] is also shown in Panel b.

Above 60 °C, the scattering functions in the low k region for PNIPAM$_{60}$-*b*-PNVP$_{368}$ (panel a) show plateaus, but those for PNIPAM$_{31}$-*b*-PNVP$_{120}$ (panel b) keep increasing with decreasing k, although some plateaus are observed in an intermediate k region above 70 °C. In panel b, the scattering function for PNIPAM$_{100}$-*b*-PNVP$_{218}$ at 60 °C obtained in the previous study[14] also keeps increasing in the low k region. The difference in the scattering function in the low k region indicates the different morphologies of the aggregating component of the block copolymers upon heating.

III-4-2. Theoretical Scattering Functions

As mentioned above, depending on the composition and degree of polymerization, the block copolymer in solution may form the micelle or undergo the liquid−liquid phase separation.

For the aqueous solution of PNIPAM-*b*-PNVP, the macroscopic phase separation does not occur, but the separated concentrated phase forms colloidal spheres or droplets in the phase separating solution.[14] Thus, the aqueous PNIPAM-*b*-PNVP solution contains the single chain, micelle, and/or colloidal sphere of the concentrated phase as scattering components. When weight fractions of the single chain, micelle, and sphere are denoted as w_{chain}, w_{mic}, and w_{sph}, respectively, and (weight average) aggregation numbers of the micelle and sphere as m_{mic} and $m_{\mathrm{w,sph}}$, respectively, the scattering function for the aqueous PNIPAM-*b*-PNVP solution may be written as[21]

$$\frac{R_{\theta,\mathrm{X}}}{K_{\mathrm{e}}c} = M_1\left[\frac{w_{\mathrm{chain}}P_{\mathrm{chain}}(k)}{1+2A_2M_1P_{\mathrm{chain}}(k)w_{\mathrm{chain}}c} + w_{\mathrm{mic}}m_{\mathrm{mic}}P_{\mathrm{mic}}(k) + w_{\mathrm{sph}}m_{\mathrm{w,sph}}P_{\mathrm{sph}}(k)\right] \quad \text{(III-12)}$$

where M_1 and A_2 are the molecular weight and the second virial coefficient of the single chain and $P_{\mathrm{chain}}(k)$, $P_{\mathrm{mic}}(k)$, and $P_{\mathrm{sph}}(k)$ are the particle scattering function of the single chain, micelle, and sphere, respectively. We consider the interparticle interference effect only among single chains in eq III-12. In what follows, M_{w} listed in Table III-1 (the last column) is used as M_1. The particle scattering function $P_{\mathrm{chain}}(k)$ of the PNIPAM-*b*-PNVP single chain, taking the random coil conformation, is expressed by[22]

$$\gamma_{\mathrm{av}}{}^2P_{\mathrm{chain}}(k) = w_{\mathrm{A}}{}^2\gamma_{\mathrm{A}}{}^2P_{\mathrm{A}}(k) + w_{\mathrm{B}}{}^2\gamma_{\mathrm{B}}{}^2P_{\mathrm{B}}(k) + 2w_{\mathrm{A}}w_{\mathrm{B}}\gamma_{\mathrm{A}}\gamma_{\mathrm{B}}Q_{\mathrm{AB}}(k) \quad \text{(III-13)}$$

with

$$P_{\mathrm{A}}(k) = 2\frac{\mathrm{e}^{-X_{\mathrm{A}}}-1+X_{\mathrm{A}}}{X_{\mathrm{A}}{}^2},\ P_{\mathrm{B}}(k) = 2\frac{\mathrm{e}^{-X_{\mathrm{B}}}-1+X_{\mathrm{B}}}{X_{\mathrm{B}}{}^2},\ Q_{\mathrm{AB}} = \frac{\left(1-\mathrm{e}^{-X_{\mathrm{A}}}\right)\left(1-\mathrm{e}^{-X_{\mathrm{B}}}\right)}{X_{\mathrm{A}}X_{\mathrm{B}}} \quad \text{(III-14)}$$

$$X_{\mathrm{A}} \equiv \tfrac{1}{6}b_{\mathrm{A}}{}^2N_{0,\mathrm{A}}k^2,\ X_{\mathrm{B}} \equiv \tfrac{1}{6}b_{\mathrm{B}}{}^2N_{0,\mathrm{B}}k^2 \quad \text{(III-15)}$$

Here, the subscripts A and B stand for PNVP and PNIPAM, respectively, b_{i} and $N_{0,\mathrm{i}}$ (i = A, B) are the effective monomer unit length and the degree of polymerization, respectively, and w_{A} and w_{B}

are the weight fractions of the A and B block chains in the copolymer chain, respectively, calculated by

$$w_{\mathrm{B}} = 1 - w_{\mathrm{A}} = \frac{M_{0,\mathrm{NIPAM}} N_{0,\mathrm{n}}(\mathrm{PNIPAM})}{M_{0,\mathrm{NVP}} N_{0,\mathrm{n}}(\mathrm{PNVP}) + M_{0,\mathrm{NIPAM}} N_{0,\mathrm{n}}(\mathrm{PNIPAM})} \tag{III-16}$$

See also eqs III-10 and 11. In what follows, $N_{0,\mathrm{n}}$(PNVP) and $N_{0,\mathrm{n}}$(PNIPAM) listed in Table III-1 are used for $N_{0,\mathrm{A}}$ and $N_{0,\mathrm{B}}$.

The particle scattering function for the spherical micelle $P_{\mathrm{mic}}(k)$ is given by[23–25]

$$\gamma_{\mathrm{av}}{}^2 P_{\mathrm{mic}}(k) = \left[\gamma_{\mathrm{A}} w_{\mathrm{A}} E_{\mathrm{A}}(k) + \gamma_{\mathrm{B}} w_{\mathrm{B}} E_{\mathrm{B}}(k)\right]^2 \mathrm{e}^{-\sigma^2 k^2} + \frac{\left(\gamma_{\mathrm{A}} w_{\mathrm{A}}\right)^2}{f}\left[P_{\mathrm{A}}(k) - E_{\mathrm{B}}{}^2(k)\right] \tag{III-17}$$

where

$$E_{\mathrm{A}}(k) = \frac{1 - \mathrm{e}^{-X_{\mathrm{A}}}}{X_{\mathrm{A}}} \frac{\sin\left[\left(R_{\mathrm{core}} + \frac{1}{6} b_{\mathrm{corona}} N_{0,\mathrm{A}}{}^{1/2}\right)k\right]}{\left(R_{\mathrm{core}} + \frac{1}{6} b_{\mathrm{corona}} N_{0,\mathrm{A}}{}^{1/2}\right)k}, \quad E_{\mathrm{B}} = 3\frac{\sin\left(R_{\mathrm{core}}k\right) - Rk\cos\left(R_{\mathrm{core}}k\right)}{\left(R_{\mathrm{core}}k\right)^3} \tag{III-18}$$

with the width σ of the core–corona interface, the bond length b_{corona} of the coronal (PNVP) chain, and the radius R_{core} of the spherical core, given by

$$\frac{4\pi}{3} R_{\mathrm{core}}{}^3 c_{\mathrm{core}} = \frac{m_{\mathrm{mic}} M_{0,\mathrm{NIPAM}} N_{0,\mathrm{PNIPAM}}}{N_{\mathrm{a}}} \tag{III-19}$$

Here, c_{core} is the PNIPAM block chain mass concentration inside the core and N_{a} is the Avogadro constant. The cylindrical micelle and vesicle are not expected for our PNIPAM-*b*-PNVP samples because $N_{0,\mathrm{n}}$(PNVP) > $N_{0,\mathrm{n}}$(PNIPAM) (cf. Table III-1).[26]

At last, the scattering function for polydisperse spheres $P_{\mathrm{sph}}(k)$ is given by[14]

$$m_{\mathrm{w,sph}} P_{\mathrm{sph}}(k) = \frac{1}{\sqrt{2\pi \ln Đ}} \int \left[3\frac{\sin\left(Rk\right) - Rk\cos\left(Rk\right)}{\left(Rk\right)^3}\right]^2 \exp\left[-\frac{\ln^2\left(\sqrt{Đ} m_{\mathrm{sph}} / m_{\mathrm{w.sph}}\right)}{2\ln Đ}\right] \mathrm{d}m_{\mathrm{sph}} \tag{III-20}$$

where $Đ$ and $m_{\mathrm{w,sph}}$ are the dispersity index and the weight average aggregation number of the spherical particles, respectively, and R_{sph} is the radius of the sphere with the aggregation number

m_{sph}, calculated by

$$\frac{4\pi}{3}R^3 c_{in} = \frac{M_1 m_{sph}}{N_a} \quad \text{(III-21)}$$

with the copolymer mass concentration c_{in} inside the spherical particle.

III-4-3. Fitting of SAXS Profiles.

Figure III-4 shows the fitting result by eqs III-12−21, for example, of the scattering function for $PNIPAM_{31}$-*b*-$PNVP_{120}$ at 73 °C. The red solid curve indicates the total theoretical scattering function, and the three black solid curves display the theoretical scattering functions of the three scattering components. The scattering components of the single chain, micelle, and polydisperse spheres mainly contribute to the total scattering function in the high *k*, intermediate *k*, and low *k* regions, respectively. Although there are many fitting parameters in the above-mentioned theoretical scattering function, the parameters for each scattering component can be determined almost uniquely by the fitting of the experimental scattering function in the corresponding *k* regions.

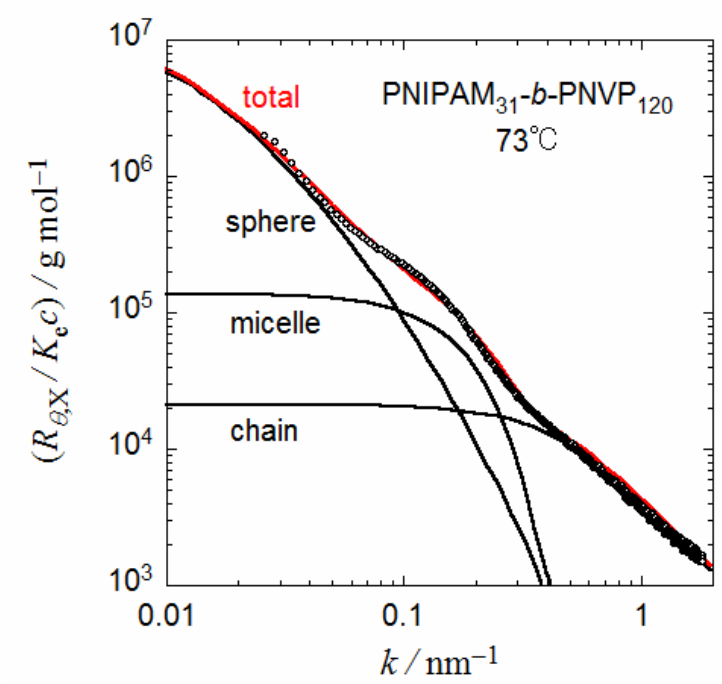

Figure III-4. The fitting result of the SAXS profile of PNIPAM$_{31}$-*b*-PNVP$_{120}$ at 73 °C. Circles, experimental data; black solid curves, theoretical scattering functions for the single chain, micelle, and polydisperse spheres components; red solid curve, total theoretical scattering function of the three scattering components.

Experimental scattering functions for PNIPAM$_{60}$-*b*-PNVP$_{368}$ and PNIPAM$_{31}$-*b*-PNVP$_{120}$ at different temperatures, as well as PNIPAM$_{100}$-*b*-PNVP$_{218}$ at 60 °C obtained previously,[14] are similarly fitted to the above equations, as shown by curves in Figure III-5, and the fitting parameters used are listed in the Table III-A of the Appendix. Scattering functions for both copolymers at 25 °C are fitted by the single-chain scattering function (dashed curves) in high *k* regions, but the upswing of the scattering functions indicates the existence of large aggregates in the solutions.[14] Although both scattering functions at 25 °C are fitted by the dotted curves for the single chain + polydisperse spheres over the whole *k* region in Figure III-5, similar fitting can be made also by the model of the single chain + random aggregate.[14]

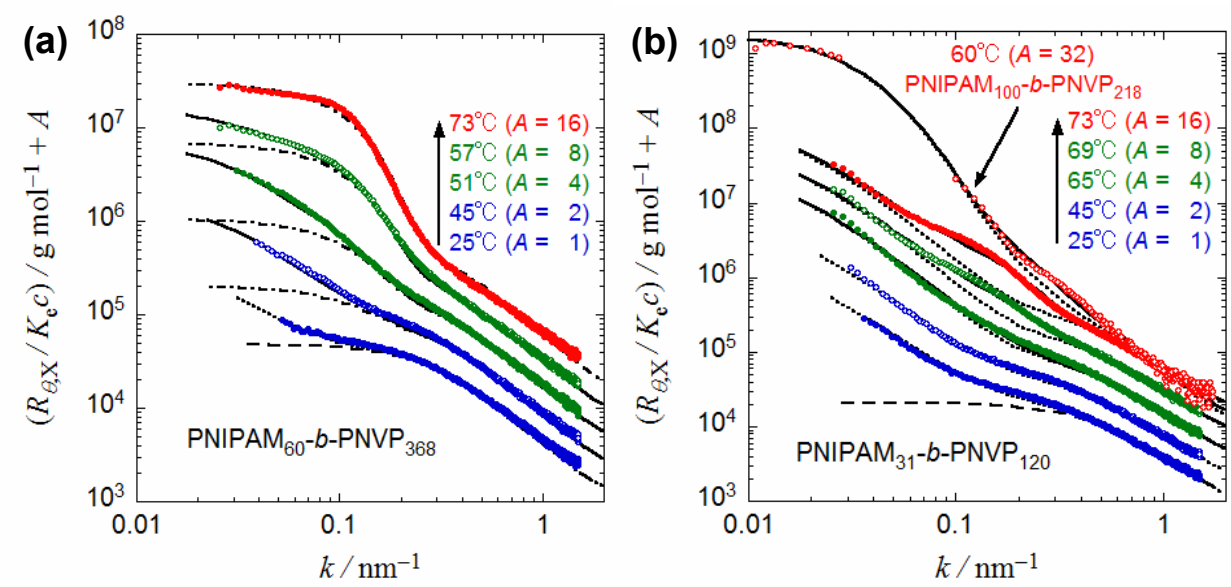

Figure III-5. Fits of experimental scattering functions for PNIPAM$_{60}$-*b*-PNVP$_{368}$ (a) and PNIPAM$_{31}$-*b*-PNVP$_{120}$ (b) at different temperatures, as well as PNIPAM$_{100}$-*b*-PNVP$_{218}$ at 60 °C obtained previously (in panel b), by eqs III-12−21. The dot-dash, dotted, and solid curves as well as the thin dashed curve indicate theoretical scattering functions for the single chain + micelle, the single chain + polydisperse spheres, the single chain + micelle + polydisperse spheres, as well as the single chain, respectively. For the viewing clarity, the scattering functions except at 25 °C shift vertically by the factor *A*.

With increasing temperature, the scattering function for PNIPAM$_{60}$-*b*-PNVP$_{368}$ in panel a in Figure III-5 grows in both the intermediate and low *k* regions, which indicates the formation of the micelle and polydisperse spheres (the concentrated phase droplets). In the panel, dash-dot and solid curves display theoretical scattering functions for the single chain + micelle and for the three scattering components, respectively. At 73 °C, the experimental scattering function can be fitted by the dash-dot curve for the single chain + micelle.

The scattering function for PNIPAM$_{31}$-*b*-PNVP$_{120}$ in panel b grows first in the low *k* region and then in both the intermediate and low *k* regions with increasing temperature. The dotted and solid curves indicate theoretical scattering functions for the single chain +

polydisperse spheres and for the three scattering components, respectively. The solid curves fit better than the dotted curves. The scattering function for PNIPAM$_{100}$-*b*-PNVP$_{218}$ at 60 °C obtained previously[14] is also fitted by the three scattering components model. The function in the intermediate *k* region indicates the existence of a small amount of the micelle for this copolymer sample, although the scattering function of this sample was previously fitted by the theoretical curve for the single chain + polydisperse spheres.[14]

Weight fractions of the single chain (w_{chain}), micelle (w_{mic}), and polydisperse spheres (w_{sph}) obtained by the above fittings are plotted against the temperature in Figure III-6. As mentioned above, the three components contribute to the SAXS scattering function at different *k* regions, so that we can determine the weight fractions accurately (within ca. 10% error). The weight fraction w_{sph} is small for both PNIPAM$_{60}$-*b*-PNVP$_{368}$ and PNIPAM$_{31}$-*b*-PNVP$_{120}$ even at temperatures where the experimental scattering functions show the upswing at low *k*. This is because the scattering power of large spheres is very strong. For PNIPAM$_{60}$-*b*-PNVP$_{368}$ with x = 0.14, w_{mic} and w_{chain} start increasing and decreasing, respectively, above 50 °C, and the concentrated phase droplet is not practically formed over the entire temperature range investigated. As seen from Table III-A(a) in the Appendix, w_{sph} takes a maximum around 55 °C and tends to zero at higher temperature. This temperature dependence of w_{sph} can be qualitatively explained by the arrows in the phase diagrams in panels a, b, e, and f of Figure III-2. The interaction parameter χ_{BS} between PNIPAM and water should increase with increasing temperature, and thus, the heating of a dilute solution corresponds to the changes along the vertical arrows indicated in Figure III-2. The solution passes through the liquid−liquid phase separation region and then goes into the micellization region. Although the theoretical phase diagram does not predict the coexistence of the concentrated-phase droplet and the micelle in the

intermediate χ_{BS} (temperature) range, the phase boundary between the liquid−liquid phase separation and micellization regions in the phase diagram should be regarded as the crossover between different self-association states of the block copolymer, as mentioned in the above theoretical section.

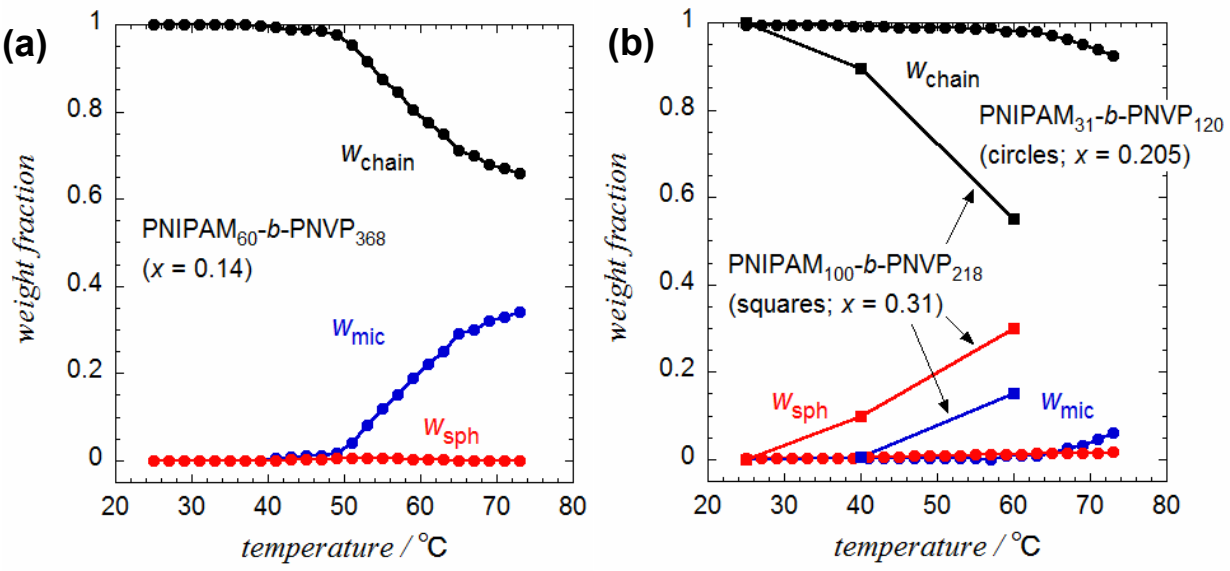

Figure III-6. Temperature dependences of the weight fractions of the single chain (black symbols), spherical micelle (blue symbols), and polydisperse spheres (red symbols) for sample PNIPAM$_{60}$-*b*-PNVP$_{368}$ (x = 0.14) (a) and samples PNIPAM$_{31}$-*b*-PNVP$_{120}$ (x = 0.205) and PNIPAM$_{100}$-*b*- PNVP$_{218}$ (x = 0.31) (b).

For PNIPAM$_{31}$-*b*-PNVP$_{120}$ with x = 0.205 and a low degree of polymerization of 151, w_{chain} starts decreasing only above 60 °C. This is consistent with the theoretical phase diagrams in Figure III-2d−f, where the binodal and micellization curves go up and the one-phase region is enlarged with decreasing P at fixed x_B. For PNIPAM$_{100}$-*b*-PNVP$_{218}$ with x = 0.31 and a degree of polymerization of 318, both w_{sph} and w_{mic} increase above 40 °C and w_{sph} is larger than w_{mic}. Thus, it turns out that the ratio w_{mic}/w_{sph} increases with decreasing x. This corresponds to the theoretical results shown in Figure III-2a−c, where the liquid−liquid phase separation region becomes

narrower and the micellization region is enlarged with decreasing x_B.

Because the lattice theory is a semiquantitative theory, we do not make a quantitative comparison between the theoretical phase diagrams in Figure III-2 and the experimental results shown in Figure III-6.

III-5. Conclusions

The competition between the micellization and liquid−liquid phase separation was investigated for dilute aqueous solutions of the thermosensitive PNIPAM-*b*-PNVP block copolymers with different degrees of polymerization of the PNIPAM and PNVP block chains upon heating by SAXS. The scattering profiles obtained were analyzed in terms of the three scattering components model consisting of the single chain, micelle, and polydisperse spheres to estimate weight fractions of the three components. When the NIPAM content is high, the liquid−liquid phase separation is superior to the micellization (or the weight fraction of the concentrated-phase droplet is larger than that of the micelle), whereas at lower NIPAM contents, the micellization is preferred to the liquid−liquid phase separation. When the total degree of polymerization of PNIPAM-*b*-PNVP is lower, the micellization and liquid−liquid phase separation occur at higher temperatures. These degrees of polymerization dependences were semiqualitatively explained by the theory based on the lattice model.

References

1. Zhang, L.; Eisenberg, A. *Science* **1995**, *268*, 1728−1731.
2. Zhang, L.; Yu, K.; Eisenberg, A. *Science* **1996**, *272*, 1777−1779.
3. Discher, D. E.; Eisenberg, A. *Science* **2002**, *297*, 967−973.
4. Mai, Y.; Eisenberg, A. *Chem. Soc. Rev*. **2012**, *41*, 5969−5985.
5. Antonietti, M.; Heinz, S.; Schmidt, M.; Rosenauer, C. *Macromolecules* **1994**, *27,*

3276−3281.

6. Förster, S.; Antonietti, M. *Adv. Mater*. **1998**, *10*, 195−217.
7. Topp, M. D. C.; Dijkstra, P. J.; Talsma, H.; Feijen, J. *Macromolecules* **1997**, *30*, 8518−8520.
8. Zhu, P. W.; Napper, D. H. *Macromolecules* **1999**, *32*, 2068−2070.
9. Sugihara, S.; Kanaoka, S.; Aoshima, S. *Macromolecules* **2005**, *38*, 1919−1927.
10. Yusa, S.; Yamago, S.; Sugahara, M.; Morikawa, S.; Yamamoto, T.; Morishima, Y. *Macromolecules* **2007**, *40*, 5907−5915.
11. Mendrek, S.; Mendrek, A.; Adler, H.-J.; Dworak, A.; Kuckling, D. *Colloid Polym. Sci.* **2010**, *288*, 777−786.
12. Weber, C.; Hoogenboom, R.; Schubert, U. S. *Prog. Polym. Sci*. **2012**, *37*, 686−714.
13. Takahashi, R.; Sato, T.; Terao, K.; Qiu, X.-P.; Winnik, F. M. *Macromolecules* **2012**, *45*, 6111−6119.
14. Sato, T.; Tanaka, K.; Toyokura, A.; Mori, R.; Takahashi, R.; Terao, K.; Yusa, S. *Macromolecules* **2013**, *46*, 226−235.
15. Takahashi, R.; Qiu, X.-P.; Xue, N.; Sato, T.; Terao, K.; Winnik, F. M. *Macromolecules* **2014**, *47*, 6900−6910.
16. Sato, T.; Takahashi, R. *Polym. J.* **2017**, *49*, 273−277.
17. Flory, P. J. *Principles of Polymer Chemistry*; Cornell Univ. Press: Ithaca, NY, 1953.
18. Hong, K. M.; Noolandi, J. *Macromolecules* **1983,** *16*, 1083−1093.
19. Shimizu, N.; Yatabe, K.; Nagatani, Y.; Saijyo, S.; Kosuge, T.; Igarashi, N. *AIP Conf. Proc.* **2015**, *1741*, 050017.
20. Takahashi, R.; Sato, T.; Terao, K.; Yusa, S. *Macromolecules* **2015**, *48*, 7222−7229.
21. Sato, T.; Jinbo, Y.; Teramoto, A. *Polym. J.* **1999**, *31*, 285−292.
22. Benoit, H.; Froelich, D. *In Light Scattering from Polymer Solutions*; Huglin, M. B., Ed.; Academic Press: London and New York, 1972; pp 467−501.
23. Pedersen, J. S.; Gerstenberg, M. C. *Macromolecules* **1996**, *29*, 1363−1365.
24. Pedersen, J. S. *J. Appl. Crystallogr.* **2000**, *33*, 637−640.
25. Bang, J.; Jain, S.; Li, Z.; Lodge, T. P.; Pedersen, J. S.; Kesselman, E.; Talmon, Y. *Macromolecules* **2006**, *39*, 1199−1208.
26. Shen, H.; Eisenberg, A. *Macromolecules* **2000**, *33*, 2561−2572.

27. Hickl, P.; Ballauff, M.; Scherf, U.; Müllen, K.; Lindner, P. *Macromolecules* **1997**, *30*, 273-279.
28. Terao, T.; Mizuno, K.; Murashima, M.; Kita, Y.; Hongo, C.; Okuyama, K.; Norisuye, T.; Bächinger, H. P. *Macromolecules* **2008**, *41*, 7203-7210.
29. Arakawa, S.; Terao, K.; Kitamura, S.; Sato, T. *Polym. Chem*. **2012**, *3*, 472-478.

Appendix.

The following Tables list fitting parameters obtained by fitting experimental SAXS profiles for three PNIPAM-*b*-PNVP samples in water at different temperatures by the theoretical scattering function explained in the text (eqs 12-21). For the single chain, the effective bond length b for PNIPAM may be underestimated by the chain thickness effect on the scattering function.[1-3] The second virial coefficient A_2 was chosen to be 1×10^{-4}, 2×10^{-5}, and 0 cm^3mol/g^2 for $PNIPAM_{60}$-*b*-$PNVP_{368}$, $PNIPAM_{31}$-*b*-$PNVP_{120}$, and $PNIPAM_{100}$-*b*-$PNVP_{218}$, respectively.

Table III-A. Values of fitting parameters for the single chain, micelle, and polydisperse spheres determined by fits of eqs III-12-21 to the experimental SAXS scattering profiles for (a) $PNIPAM_{60}$-*b*-$PNVP_{368}$, (b) $PNIPAM_{31}$-*b*-$PNVP_{120}$, and (c) $PNIPAM_{100}$-*b*-$PNVP_{218}$.

(a) $PNIPAM_{60}$-*b*-$PNVP_{368}$ ($x = 0.14$)

	25 °C	35 °C	45 °C	55 °C	65 °C	73 °C
w_{chain} [a]	0.999	0.999_5	0.987	0.875	0.71	0.66
b(PNVP)/nm [b]	0.67	0.67	0.67	0.67	0.67	0.67
b(PNIPAM)/nm [b]	0.1	0.1	0.1	0.1	0.1	0.1
w_{mic} [a]	0	0	0.01	0.12	0.29	0.34
m_{mic} [c]	–	–	90	90	90	90
c_{core} / g cm^{-3} [d]	–	–	1.0	1.0	1.0	1.0
b_{corona}/nm [b]	–	–	0.7	0.7	0.7	0.7
$(\sigma/nm)^2$ [e]	–	–	7	7	7	7
w_{sph} [a]	0.001	0.0005	0.0028	0.005	0	0
$m_{w,sph}$ [c]	4000	4000	4000	4000	–	–
$Đ$ [f]	10	10	10	10	–	–
c_{in} / g cm^{-3} [d]	1.0	1.0	1.0	1.0	–	–

(b) $PNIPAM_{31}$-*b*-$PNVP_{120}$ (x = 0.205)

	25 °C	35 °C	45 °C	55 °C	65 °C	73 °C
w_{chain} [a]	0.997	0.986	0.983_5	0.979_5	0.967_5	0.924
b(PNVP)/nm [b]	0.67	0.67	0.67	0.67	0.67	0.68
b(PNIPAM)/nm [b]	0.2	0.2	0.2	0.2	0.2	0.2
w_{mic} [a]	0	0.0095	0.0095	0.01	0.018	0.060
m_{mic} [c]	–	100	100	100	110	110
c_{core} / g cm^{-3} [d]	–	1.0	1.0	1.0	1.0	1.0
b_{corona}/nm [b]	–	0.67	0.67	0.67	0.67	0.67
$(\sigma/\text{nm})^2$ [e]	–	3	3	3	3	2
w_{sph} [a]	0.0033	0.0045	0.007	0.0105	0.0145	0.016
$m_{w,sph}$ [c]	4×10^4	5×10^4	5×10^4	5×10^4	5×10^4	3.5×10^4
$Đ$ [f]	1×10^4	1×10^4	1×10^4	1×10^4	1×10^4	1×10^4
c_{in} / g cm^{-3} [d]	1.05	0.6	0.6	0.5	0.5	0.65

(c) $PNIPAM_{100}$-*b*-$PNVP_{218}$ (x = 0.31)

	25 °C[14]	40 °C	60 °C
w_{chain} [a]	1.0	0.895	0.55
b(PNVP)/nm [b]	0.65	0.90	0.95
b(PNIPAM)/nm [b]	0.25	0.50	0.50
w_{mic} [a]	0	0.005	0.15
m_{mic} [c]	–	8	10
c_{core} / g cm^{-3} [d]	–	1.0	1.0
b_{corona}/nm [b]	–	0.60	0.58
$(\sigma/\text{nm})^2$ [e]	–	0.5	1.0
w_{sph} [a]	6×10^{-5} [g]	0.10	0.30
$m_{w,sph}$ [c]	7700 [g]	2.4×10^4	4300
$Đ$ [f]	–	2	6
c_{in} / g cm^{-3} [d]	–	0.40	0.50

[a] Weight fractions of the isolated chain, spherical micelle, and polydisperse sphere. [b] Effective monomer unit lengths of the PNVP block chain, the PNIPAM block chain, and coronal (PNVP) chain; b_{PNIPAM} may be underestimated by the chain thickness effect on the scattering function.[27-29] [c] Aggregation number of the spherical micelle and the weight average aggregation number of the polydisperse sphere. [d] Polymer mass concentrations inside the hydrophobic core of the micelle and the polydisperse sphere. [e] Width of the core-corona interface. [f] Dispersity index for the aggregation number of the polydisperse sphere. [g] Fitted by the randomly branching chain of tri-functional monomers. [14]

Chapter IV

Phase Separation and Micellization in Aqueous Solutions of Mixtures of PNIPAM-*b*-Poly(*N*-vinyl-2-pyrrolidone) and PNIPAM homopolymer upon Heating

IV-1. Introduction

Amphiphilic block copolymers are often utilized as emulsifiers in order to stabilize colloidal dispersions.[1-3] Solvophobic block chains of the block copolymer are adsorbed on the solvophobic surface of the colloidal particle, and solvophilic block chains of adsorbed block copolymers hinder the coagulation of colloidal particles in the solvent. However, solvophilic block chains sometimes make the colloidal particle surface soften to help the coalescence of colloidal particles, i.e., the block copolymer acts as a flocculant of colloidal dispersion.[4,5]

As discussed in Chapter II, spherical droplets formed in the phase-separating aqueous PNIPAM solution upon heating have a radius of order of 100 nm, but do not coalesce because of the hardness of the droplet surface. When the block copolymer, poly(*N*-isopropylacrylamide)-*b*-poly(*N*-vinyl-2-pyrrolidone) (PNIPAM-*b*-PNVP), is added to the aqueous PNIPAM homopolymer solution, the block copolymer may be adsorbed on the PNIPAM droplet surface. Does this adsorption of the block copolymer stabilize or destabilize colloidal dispersion of the phase-separating PNIPAM solution? If the block copolymer destabilizes the colloidal PNIAPM solution, it can be utilized as the flocculant to recover PNIPAM from its aqueous solution upon heating.

From the point of view of PNIPAM-*b*-PNVP, the addition of PNIPAM homopolymer to the block copolymer solution may affect the competition of the phase separation and

micellization. As mentioned in Chapter III, this competition depends on the composition and molecular weight of the block copolymer. The addition of the homopolymer may be another factor to control the competition.

The present Chapter investigates the phase separation and micellization behavior in aqueous solutions of mixtures of the PNIPAM homopolymer and the PNIPAM-*b*-PNVP block copolymer by macroscopic and microscopic observations and SAXS measurements, expecting that the competition between the micellization and liquid-liquid phase separation of the block copolymer can be controlled by addition of the PNIPAM homopolymer to the block copolymer solution. Experimental results obtained for the homopolymer + block copolymer mixture solutions are compared with corresponding experimental results for the homopolymer solution and block copolymer solution.

IV-2. Experimental Section

IV-2-1. Materials.

Two block copolymer samples, $PNIPAM_{60}$-*b*-$PNVP_{368}$ and $PNIPAM_{31}$-*b*-$PNVP_{120}$, used in Chapter III and one PNIPAM homopolymer sample with a degree of polymerization of 1100 ($PNIPAM_{1100}$) used in Chapter II were used also in this chapter. The block copolymers were synthesized by the organotellurium-mediated controlled radical polymerization.

Table IV-1. Molecular Characteristics of PNIPAM-*b*-PNVP and PNIPAM Sample Used in This Chapter.

sample	$N_{0,n}$(PNIPAM) [a]	$N_{0,n}$(PNVP) [a]	$N_{0,n}$	x	M_w/M_n [b]	$M_w/10^4$ [c]
$PNIPAM_{60}$-*b*-$PNVP_{368}$	60	368	428	0.14	1.25	5.95
$PNIPAM_{31}$-*b*-$PNVP_{120}$	31	120	151	0.21	1.26	2.12
$PNIPAM_{1100}$	1100	-	1100	1	1.09	13.52

[a]Determined by ^{1}H NMR. [b]Determined by SEC. [c]Weight-average molecular weights calculated by $[113N_{0,n}(\text{PNIPAM}) + 111N_{0,n}(\text{PNVP})]M_w/M_n$ using the results listed in the second, third, and sixth columns. [d]Sample used in the previous study.[6]

IV-2-2. Macroscopic and Microscopic Observations.

All the test solution were heated in a heating oven to take pictures at different heating times. The microscopic observations were carried out by an Olympus U-OPA microscopy. Test solutions were sandwiched between glass slide and cover slide, and set on a heating plate (Kitazato MP-100 MFH) to take pictures at different heating times.

IV-2-3. Small angel X-ray scattering.

Small-angle X-ray scattering (SAXS) measurements of aqueous solutions of the mixture of PNIPAM and PNIPAM-*b*-PNVP were performed by the BL40B2 beamline, SPring-8, Hyogo. The details of experimental method and heating rate are the same as those in Chapters II and III. Both concentrations of the PNIPAM-*b*-PNVP copolymer and the PNIPAM homopolymer in test solutions were fixed to 2 wt%. Thus, the total polymer concentration was 4 wt% and the weight fraction of the homopolymer w_{homo} in the total polymer was 0.5. The total polymer mass concentration c was calculated from the weight fraction multiplied by the solution density at each

temperature.

The scattering intensity was calibrated by use of an aqueous PNIPAM solution at 25 °C as the reference. The SAXS optical constant K_e was calculated by[7]

$$K_e = N_A a_e^2 \left[\left(\frac{n_{e,0}}{M_0} - \frac{\bar{\upsilon} n_{solv}}{\bar{\upsilon}_{solv} M_{solv}} \right)_{co}^2 (1 - w_{homo}) + \left(\frac{n_{e,0}}{M_0} - \frac{\bar{\upsilon} n_{solv}}{\bar{\upsilon}_{solv} M_{solv}} \right)_{homo}^2 w_{homo} \right] \quad \text{(IV-1)}$$

The notation is the same as that in Chapter II (cf. eq II-2).

IV-3. Results and Discussion

IV-3-1. Turbidity and Microscopic Observations.

As mentioned in Chapter II, when the 2 wt% aqueous PNIPAM homopolymer solution was heated to 50 ° C, PNIPAM chains mostly coagulate to form spherical droplets with a radius of ca. 100 nm. Such a large colloidal droplet has so strong light scattering power that the colloidal solution is turbid, as shown in Figure IV-1a.

On the other hand, the block copolymers, $PNIPAM_{60}$-*b*-$PNVP_{368}$ and $PNIPAM_{31}$-*b*-$PNVP_{120}$, are much less hydrophobic due to the hydrophilic PNVP block chain, and SAXS results indicated that the main component in 2wt% aqueous solution was still the single chain even at 50 °C, (cf. Figures III-3 to 6 in Chapter III). As the result, 2wt% aqueous solutions of the two block copolymers, $PNIPAM_{60}$-*b*-$PNVP_{368}$ and $PNIPAM_{31}$-*b*-$PNVP_{120}$, are not so much turbid, as demonstrated in Figure IV-1b and c. The aqueous $PNIPAM_{31}$-*b*-$PNVP_{120}$ solution in Panel c is slightly more transparent than the $PNIPAM_{60}$-*b*-$PNVP_{368}$ solution in Panel b. This is because the more hydrophobic PNIPAM block chain is shorter for the former block copolymer, and Figures III-3 to III-6 in Chapter III have demonstrated that the single chain content is higher for $PNIPAM_{31}$-*b*-$PNVP_{120}$.

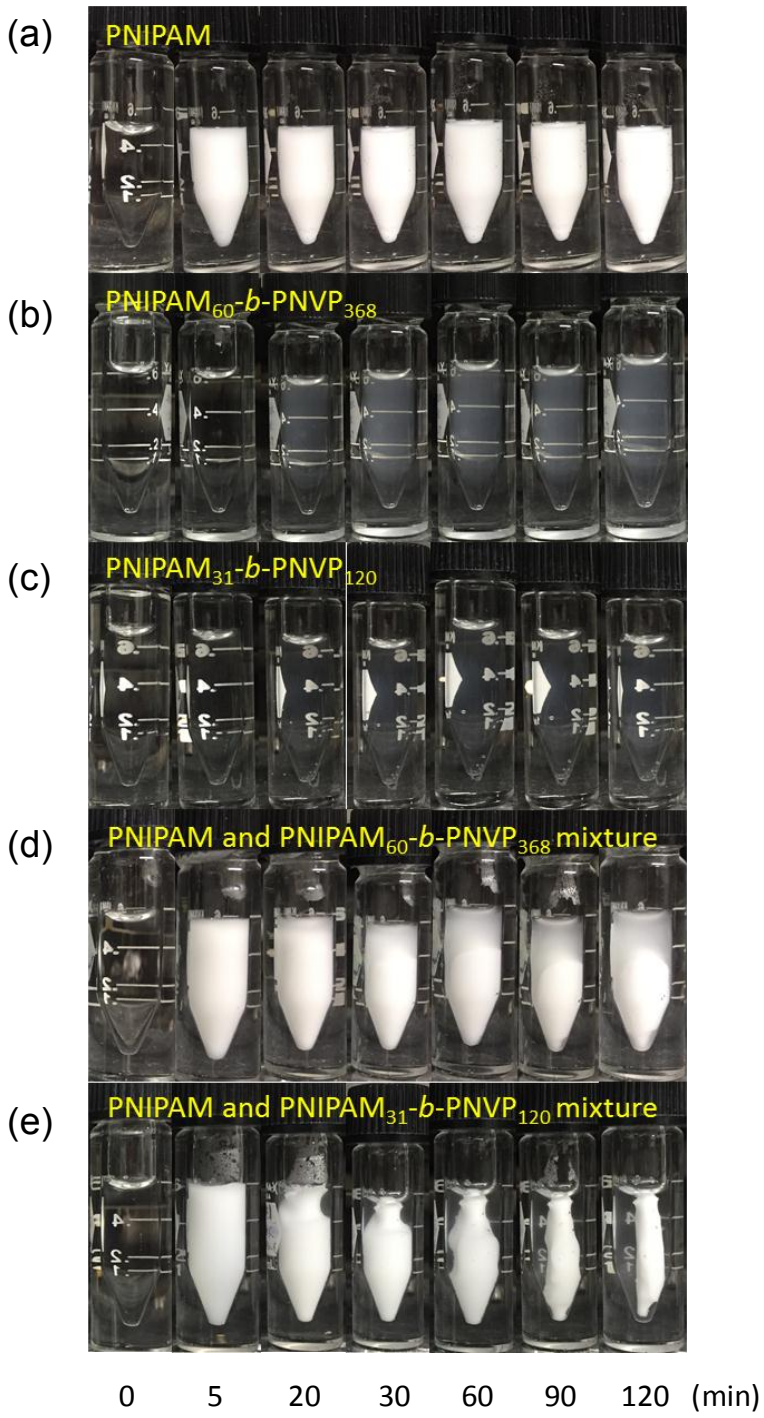

Figure IV-1. Time evolutions of the phase separation in aqueous solutions of (a) $PNIPAM_{1100}$, (b) $PNIPAM_{60}$-*b*-$PNVP_{368}$, (c) $PNIPAM_{31}$-*b*-$PNVP_{120}$, (d) the mixture of $PNIPAM_{60}$-*b*-$PNVP_{368}$ and $PNIPAM_{1100}$, as well as (e) the mixture of $PNIPAM_{31}$-*b*-$PNVP_{120}$ and $PNIPAM_{1100}$ at 50 °C. For all the solutions, the weight % concentration of the homopolymer and block copolymer were 2 wt%.

Panels d and e in Figure IV-1 display photographs of aqueous solutions containing the mixtures of $PNIPAM_{1100}$ and $PNIPAM_{60}$-*b*-$PNVP_{368}$ and of $PNIPAM_{1100}$ and $PNIPAM_{31}$-*b*-$PNVP_{120}$ at 50 °C. Both concentrations of the homopolymer and block copolymer were 2 wt%. The aqueous solution of the mixture of $PNIPAM_{1100}$ and $PNIPAM_{60}$-*b*-$PNVP_{368}$ in Panel d become turbid just after heated to 50 °C, but after keeping at 50 °C for 20 min, the turbid phase shrinks and a less turbid region appears on the top of the solution. The aqueous solution of the mixture of $PNIPAM_{1100}$ and $PNIPAM_{31}$-*b*-$PNVP_{120}$ in Panel e also become turbid just after heated to 50 °C, and then after keeping at 50 °C for 20 min, the turbid phase shrinks and an almost transparent phase appears on the side of the solution.

Tanaka[8] reported the shrinkage of the polymer-rich phase in an aqueous poly(vinyl methyl ether) (PVME) solution. He observed a network structure of the polymer-rich phase in the phase-separating solution by microscopy. The network structure shrunk as the polymer-rich phase discharged water to the surrounding matrix. To check the similarity of our solutions to his, we observed our homopolymer + block copolymer mixture solutions by an optical microscope. Figure IV-2 displays microscopic images of the homopolymer solution and the homopolymer + block copolymer mixture solutions. Although the homopolymer solution is turbid, it has no structure in the microscopic image. As mentioned in Chapter II, the homopolymer solution contains polymer-rich droplets with a radius of ca. 100 nm at 50 °C, which cannot be observed by the optical microscope. On the other hand, the phase-separating solutions containing the homopolymer + block copolymer mixtures have a network structure (the upper panel) or shrunk network structure (the bottom panel). As seen in the right panels, those structures develop rather quickly after the temperature jump to 50 °C.

The microscopic network structures in the homopolymer + block copolymer mixture

solutions resemble those observed by Tanaka[8] for aqueous PVME solutions. Therefore, the shrinkage phenomena of the polymer-rich phase observed in our solutions and Tanaka's seem to occur by a similar mechanism. Tanaka has reported a double-well-shaped phase diagram for his aqueous PVME solution, and insisted that this unique phase diagram has somethings to do with the network structure in the phase-separating solution. However, he also reported a similar unique phase separation behavior even in aqueous PNIPAM solution. The aqueous PNIPAM solution does not have such a double-well-shaped phase diagram (cf. Figure II-8), so that the relation between the shrinkage phenomena of the polymer-rich phase and the phase diagram is not still clear.

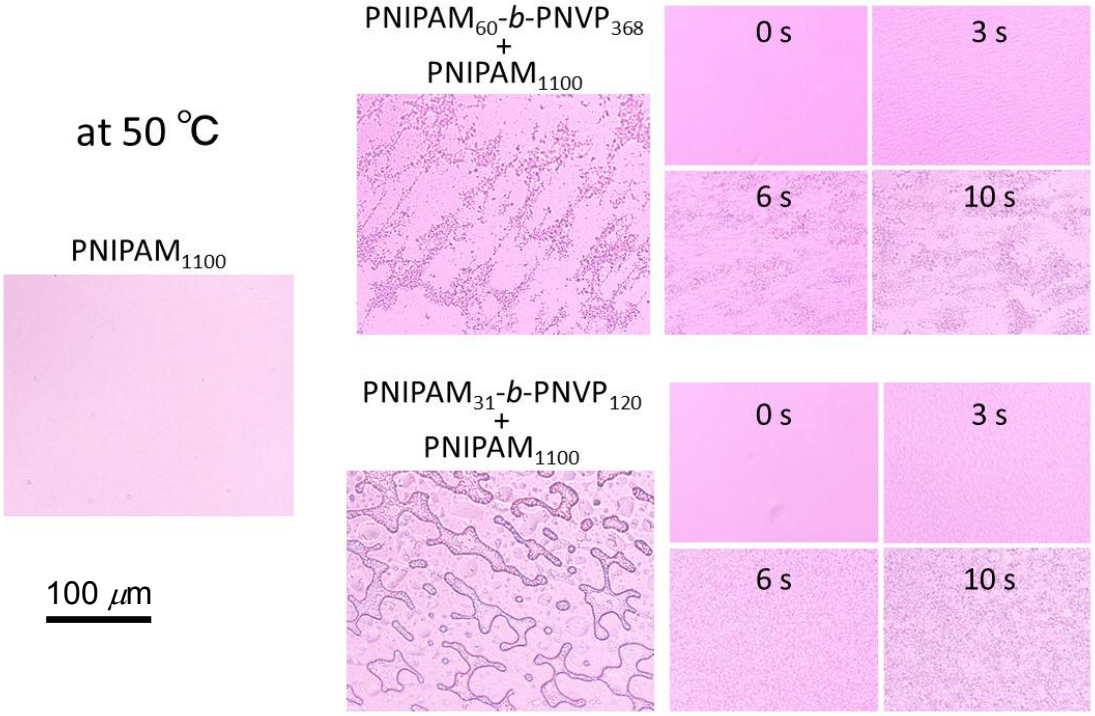

Figure IV-2. Microscopic observations of phase-separating aqueous solutions of $PNIPAM_{1100}$ (left) and of the mixtures of $PNIPAM_{1100}$ and the block copolymer, $PNIPAM_{60}$-*b*-$PNVP_{368}$ or $PNIPAM_{31}$-*b*-$PNVP_{120}$ (middle) 10 min after the temperature jump to 50 °C. Right panels show the time evolutions of the mixture solutions. For all the solutions, the weight % concentration of the homopolymer and block copolymer were 2 wt%.

IV-3.2. Small Angle X-Ray Scattering.

Figure IV-3 shows SAXS profiles for aqueous solutions of the $PNIPAM_{60}$-*b*-$PNVP_{368}$ + $PNIPAM_{1100}$ mixture (a) and of $PNIPAM_{31}$-*b*-$PNVP_{120}$ + $PNIPAM_{1100}$ mixture (b) at different temperatures. At $k < 0.05$ nm^{-1}, the intensity first increases but decreases with temperature for both mixture solutions. Data points for 37, 51, and 57 °C almost obey lines with the slope of –4, indicating that the large scattering component is the spherical particle. In Panel a, the scattering function at 73 °C exhibits a plateau in an intermediate k region (~ 0.1 nm^{-1}). This plateau resembles that of aqueous solution of $PNIPAM_{60}$-*b*-$PNVP_{368}$ alone at the same temperature (cf. Figure III-3), implying the existence of the spherical micelle component in the solution.

In the higher k region (> 0.3 nm^{-1}), the temperature dependence of the scattering function is weak for both mixture solutions. This indicates that the single chain component of the copolymer remains even at high temperatures, like the solutions of block copolymer alone (cf. Figure III-3).

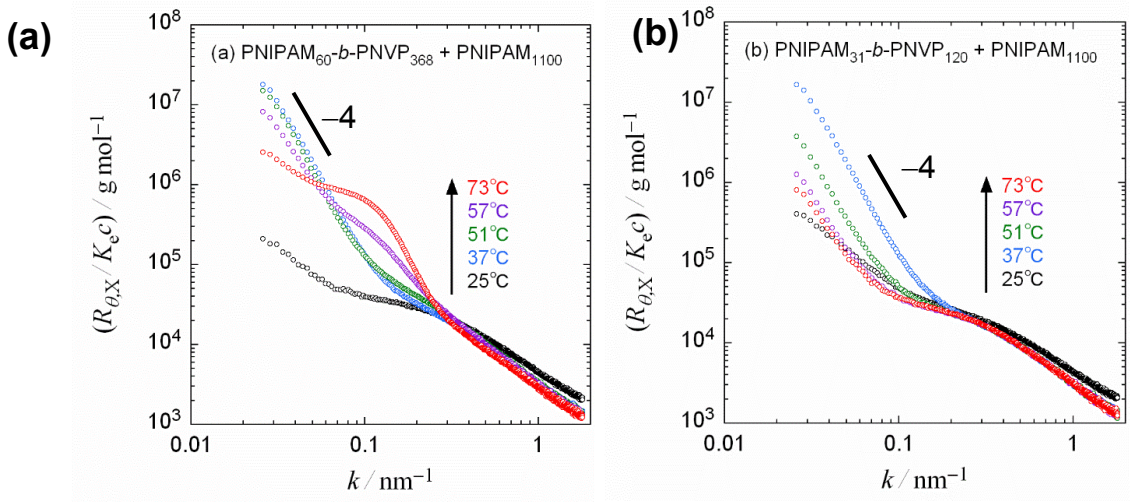

Figure IV-3. SAXS profiles for aqueous solutions of the $PNIPAM_{60}$-*b*-$PNVP_{368}$ + $PNIPAM_{1100}$ mixture (a) and of $PNIPAM_{31}$-*b*-$PNVP_{120}$ + $PNIPAM_{1100}$ mixture (b) at different temperatures.

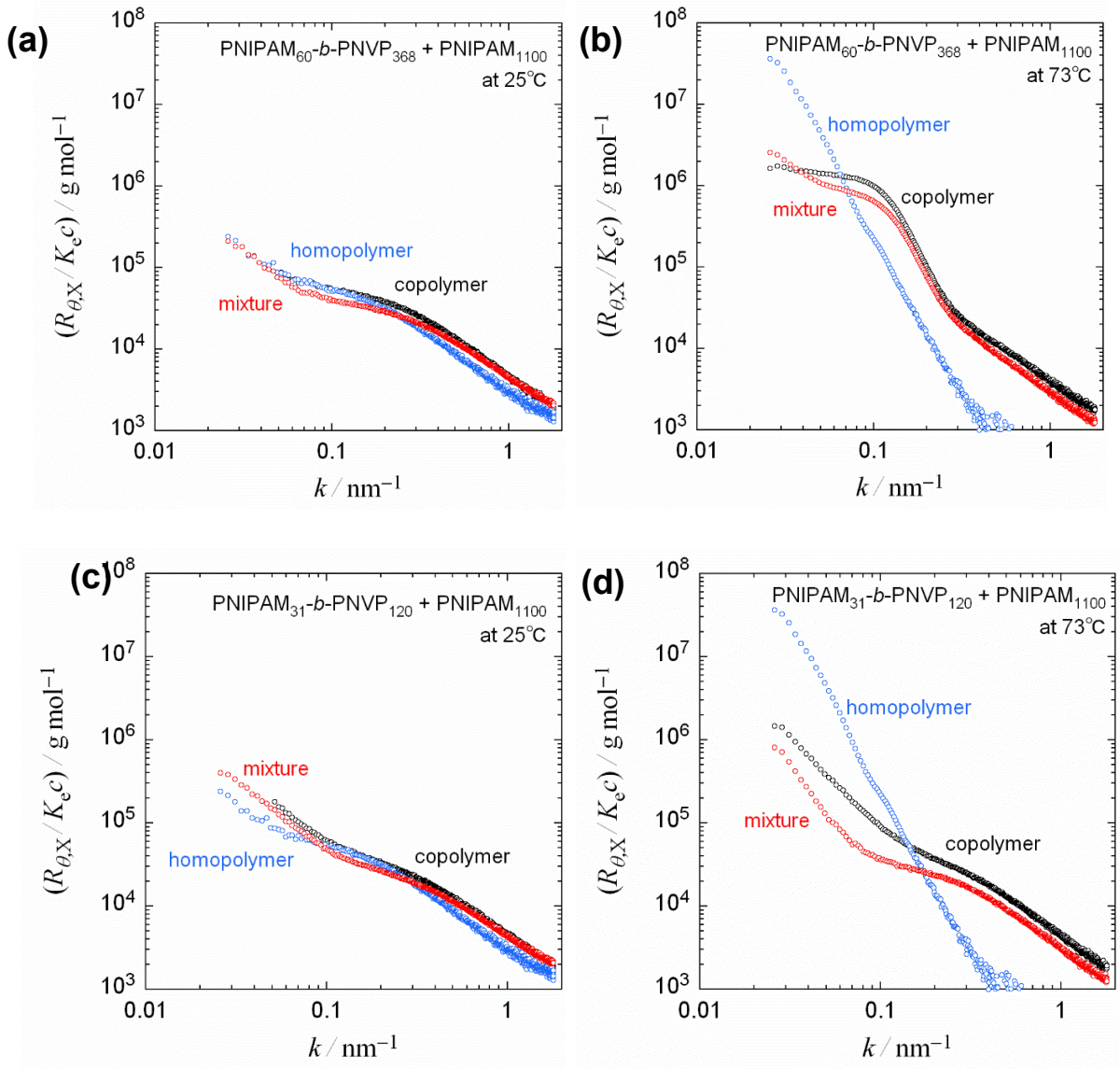

Figure IV-4. Comparison of SAXS profiles for aqueous solutions of the block copolymer + homopolymer mixtures with those for aqueous solutions of the copolymer alone and of the homopolymer alone at 25 and 73 °C. (a) and (b), the PNIPAM$_{60}$-*b*-PNVP$_{368}$ + PNIPAM$_{1100}$ mixture at 25 and 73 °C, respectively; (c) and (d), PNIPAM$_{31}$-*b*-PNVP$_{120}$ + PNIPAM$_{1100}$ mixture at 25 and 73 °C, respectively.

Figure IV-4 compares the scattering functions for aqueous solutions of the block copolymer + homopolymer mixtures with those for aqueous solutions of the copolymer alone and of the homopolymer alone at 25 and 73 °C. At 25 °C, where water is the good solvent for

both copolymer and homopolymer, the scattering function for the mixture resembles those for the copolymer and homopolymer alone. On the other hand, at 73 °C, the scattering function for the mixture resembles more that for the copolymer than that for the homopolymer.

IV-3-3. Analysis of the SAXS Profiles.

If the dispersion states of the block copolymer (component 1) and the homopolymer (component 2) in the aqueous solution do not alter by mixing, the scattering function for the mixture may be written as[9]

$$\frac{R_{\theta,X}}{K_e c} = \frac{\begin{bmatrix} \tilde{\gamma}_1^{\,2} w_1 M_1 P_1(k) + \tilde{\gamma}_2^{\,2} w_2 M_2 P_2(k) \\ +2 w_1 M_1 P_1(k) w_2 M_2 P_2(k) c\left(\tilde{\gamma}_2^{\,2} A_{11} - 2\tilde{\gamma}_1\tilde{\gamma}_2 A_{12} + \tilde{\gamma}_1^{\,2} A_{22}\right) \end{bmatrix}}{\left[1 + 2A_{11} w_1 M_1 P_1(k) c\right]\left[1 + 2A_{22} w_2 M_2 P_2(k) c\right] - 4 w_1 M_1 P_1(k) w_2 M_2 P_2(k) A_{12}^{\,2} c^2} \qquad \text{(IV-2)}$$

where w_i, M_i, and P_i (k) are the weight fraction (in the total polymer), the molar mass, and the particle scattering function of component i (= 1, 2), $\tilde{\gamma}_i$ is the excess electron density of component i relative to the averaged one, and A_{ij} is the second virial coefficient between components i and j (i, j = 1, 2), and c is the total polymer mass concentration. When w_1 = 1 (0) and w_2 = 0 (1), we obtain the scattering functions for component 1 (2) alone as

$$\left(\frac{R_{\theta,X}}{K_e c}\right)_1 = \frac{M_1 P_1(k)}{1 + 2A_{11} c_1 M_1 P_1(k)}, \quad \left(\frac{R_{\theta,X}}{K_e c}\right)_2 = \frac{M_2 P_2(k)}{1 + 2A_{22} c_2 M_2 P_2(k)} \qquad \text{(IV-3)}$$

From the above equations, we can calculate $w_i c M_i P_i$ (k) by

$$w_i c M_i P_i(k) = \frac{\left(R_{\theta,\mathrm{X}} / K_e c\right)_i}{1/\left(w_i c\right) - 2A_{ii}\left(R_{\theta,\mathrm{X}} / K_e c\right)_i} \equiv \tilde{R}_{\theta,\mathrm{X},i} \qquad \text{(IV-4)}$$

Using the experimental $(R_{\theta,\mathrm{X}}/K_e c)_i$ and A_{ii}, we can calculate $\tilde{R}_{\theta,\mathrm{X},i}$, and substituting these calculated values into eq IV-2, we can calculate the scattering function for the mixture by

$$\frac{R_{\theta,X}}{K_e c} = \frac{1}{c}\frac{\tilde{\gamma}_1^{\,2}\tilde{R}_{\theta,\mathrm{X},1} + \tilde{\gamma}_2^{\,2}\tilde{R}_{\theta,\mathrm{X},2} + 2\tilde{R}_{\theta,\mathrm{X},1}\tilde{R}_{\theta,\mathrm{X},2}\left(\tilde{\gamma}_2^{\,2}A_{11} - 2\tilde{\gamma}_1\tilde{\gamma}_2 A_{12} + \tilde{\gamma}_1^{\,2}A_{22}\right)}{\left(1+2A_{11}\tilde{R}_{\theta,\mathrm{X},1}\right)\left(1+2A_{22}\tilde{R}_{\theta,\mathrm{X},2}\right) - 4\tilde{R}_{\theta,\mathrm{X},1}\tilde{R}_{\theta,\mathrm{X},2}A_{12}^{\,2}} \qquad \text{(IV-5)}$$

if the dispersion states of both components are not altered by mixing. Only adjustable parameter in eq IV-5 is A_{12}.

Figure IV-5 compares experimental scattering functions for aqueous solutions of the block copolymer + homopolymer mixture (circles) with those calculated by eq IV-5 along with eq IV-4 (solid curves). Values of the second virial coefficients A_{11} and A_{22} used in eq IV-5 were the same as those used in Figure III-5 (Chapter III) and in Figures II-5 and II-6 (Chapter II; cf. Tables II-2 and II-4). The adjustable parameter A_{12} at 25 and 37 °C was chosen so as to give best fits (cf. Table IV-2). The solid curves agree well with the experimental results at 25 and 37 °C, demonstrating that the dispersion states of both PNIAPM homopolymer and PNIPAM-*b*-PNVP block copolymers in aqueous solution are not affected by the mixing at 25 and 37 °C. On the other hand, the solid curves 51, 57, and 73 °C do not fit to the experimental results for both mixtures with physically reasonable values of A_{12}. This indicates that the mixing of the block copolymer and homopolymer affects the dispersion states of the homopolymer and/or block copolymers.

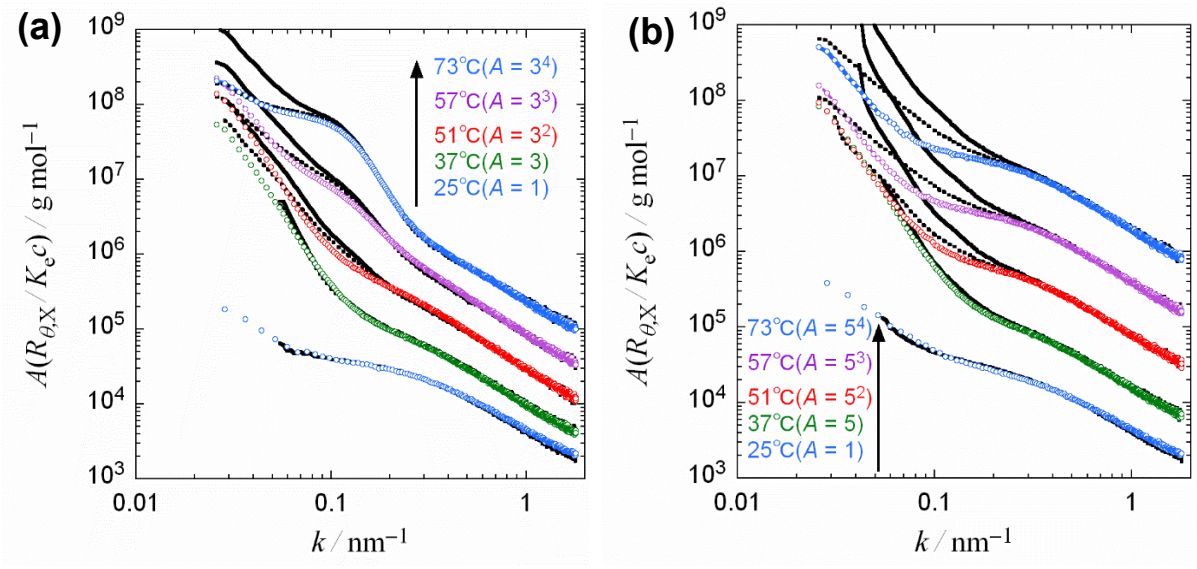

Figure IV-5. Comparison of experimental scattering functions for aqueous solutions of the block copolymer + homopolymer mixtures with those calculated by eq IV-5 along with eq IV-4 (solid curves) and with eq IV-6 (dotted curves).

Table IV-2. Parameter Values Used to Calculate the Scattering Function in Figure IV-5.

temp	$PNIPAM_{60}$-*b*-$PNVP_{368}$ + $PNIPAM_{1100}$				$PNIPAM_{31}$-*b*-$PNVP_{120}$ + $PNIPAM_{1100}$			
	A_{11} [a]	A_{22}	A_{12} [a]	ξ_2	A_{11} [a]	A_{22}	A_{12} [a]	ξ_2
25 °C	1.0	3.0 [a]	2.5	1	0.20	3.0 [a]	1.7	1
37 °C		1.0 [b]	0.25	0.9		1.0 [b]	0.1	0.8
51 °C		1.5 [b]	0	0.5		1.5 [b]	0.1	0.18
57 °C		2.0 [b]	0	0.3		2.0 [b]	0	0
73 °C		0.3 [b]	0	0.1		0.3 [b]	0	0

[a] In units of 10^{-4} $cm^3g^{-2}mol$. [b] In units of 10^{-8} $cm^3g^{-2}mol$.

As shown in Chapter II (Table II-4), the aqueous solution of the $PNIPAM_{1100}$ homopolymer contains droplets with the weight average molar mass of (3–7) × 10^8 g/mol and the average

radius of 100−130 nm above 35 °C. As displayed in Figures IV-1 and IV-2, the colloidal droplets of the PNIPAM homopolymer in water coalesce to form larger particles (or network structure) upon addition of the PNIPAM-*b*-PNVP block copolymer. When the spherical droplet size increases, the particle scattering function $P_2(k)$ diminishes very much, as demonstrated in Figure IV-6. Thus, $\tilde{R}_{\theta,\mathrm{X},2}$ in eq IV5 must be reduced from the value calculated by IV-4.

Furthermore, the shrinkage of the polymer-rich phase shown in Figure IV-1e makes the test solution of the SAXS experiment inhomogeneous. Figure IV-7 shows the aqueous solution of the $\mathrm{PNIPAM_{31}}$-*b*-$\mathrm{PNVP_{120}}$ + $\mathrm{PNIPAM_{1100}}$ mixture at 45 °C in the capillary set horizontally in the SAXS cell holder. While the solution in the capillary is uniform and transparent before the temperature jump (0 min), after the temperature jump it becomes turbid (5 – 30 min), and then the macroscopic phase separation takes place (60 and 120 min). Thus, X-ray used in the SAXS experiment does not pass though the homogeneous solution. This phase separation makes also $\tilde{R}_{\theta,\mathrm{X},2}$ diminish.

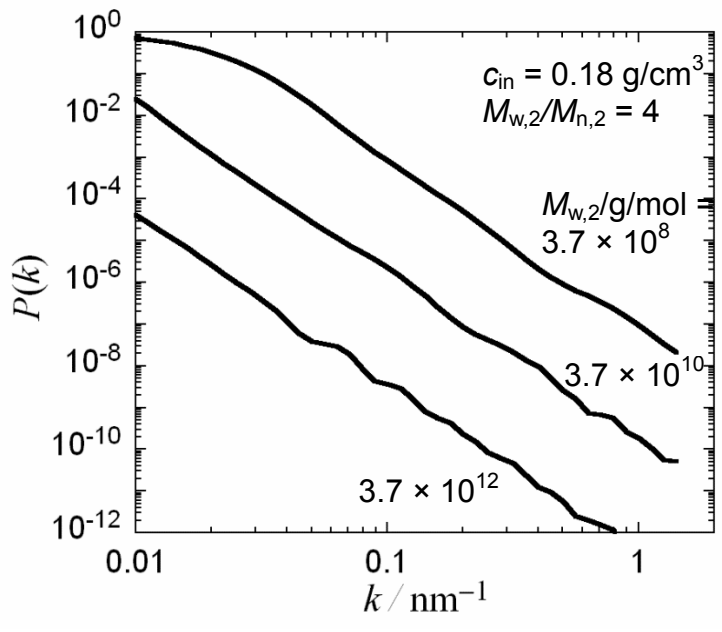

Figure IV-6. Particle scattering function for polydisperse spheres with different particle sizes.

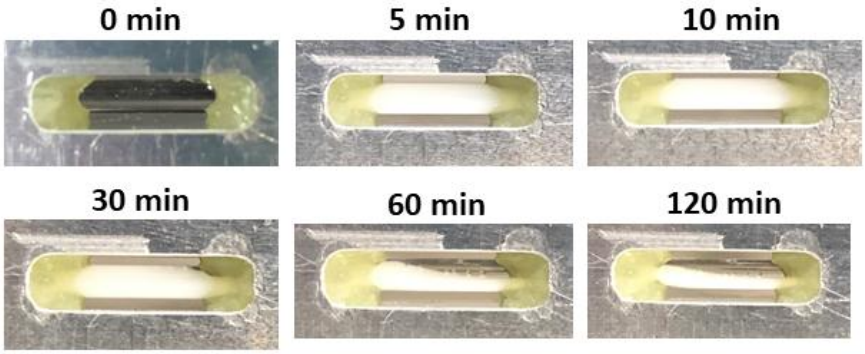

Figure IV-7. Shrinkage of the polymer-rich phase in the aqueous solution of the $PNIPAM_{31}$-*b*-$PNVP_{120}$ + $PNIPAM_{1100}$ mixture at 45 °C in the capillary set in the SAXS cell holder horizontally.

To take into account these effects, $\tilde{R}_{\theta,\mathrm{X},2}$ is reduced by a factor ξ_2

$$\tilde{R}_{\theta,\mathrm{X},2} = \frac{\left(R_{\theta,\mathrm{X}}/K_{\mathrm{e}}c\right)_2 \xi_2}{1/\left(w_2 c\right) - 2A_{22}\left(R_{\theta,\mathrm{X}}/K_{\mathrm{e}}c\right)_2} \tag{IV-6}$$

Dotted curves, indicating theoretical values calculated by eq IV-5 along with eq IV-6 using values of the factor ξ_2 listed in Table IV-2, are much closer to the experimental results in a low k region (< 0.2 nm^{-1}). The ξ_2 value chosen for the $PNIPAM_{31}$-*b*-$PNVP_{120}$ + $PNIPAM_{1100}$ mixture at each temperature (> 25 °C) is smaller than that for the $PNIPAM_{60}$-*b*-$PNVP_{368}$ + $PNIPAM_{1100}$ mixture, which corresponds to the enhancement of the macroscopic phase separation in the former mixture solutions (cf. Figures IV-1 and IV-2).

However, the dotted curves at 51, 57, and 73 °C exhibit weaker k dependences in the low k region for both mixtures. As shown in Figure IV-6, the growth of the spherical droplet makes the k dependence stronger in a low k region (k < 0.04 nm^{-1}), where the dotted curves and experimental results do not agree with each other. Therefore, the spherical droplet component

formed by the block copolymer (component 1) may also grow by addition of the PNIPAM homopolymer. It is possible that the block copolymer and the homopolymer are mixed to form larger spherical droplets in both mixture solutions above 50 °C.

The dotted curve for the $PNIPAM_{60}$-*b*-$PNVP_{368}$ + $PNIPAM_{1100}$ mixture at 73 °C almost agrees with the experimental scattering function over the entire *k* region examined. This block copolymer do not practically forms the spherical droplet component in water at 73 °C (cf. Table III-A in the Appendix of Chapter III), so that the above-mentioned effect on the spherical droplet component does not affect the scattering function at 73 °C in the low *k* region. This demonstrates that the hydrophobic core of the spherical micelle formed by the block copolymer does not contain the PNIPAM homopolymer in the mixture solution at the high temperature. The experimental scattering functions for the same mixture solution at 51 and 57 °C as well as those for the $PNIPAM_{31}$-*b*-$PNVP_{120}$ + $PNIPAM_{1100}$ mixture at 51, 57, and 73 °C do not exceed the corresponding dotted curves, indicating that the molar mass of the spherical micelle component formed of the block copolymers does not increase by addition of the PNIPAM homopolymer, and thus the micelle also does not contain the PNIPAM homopolymer.

IV-4. Concluding Remarks

As concluded in Chapters II and III, while spherical polymer-rich droplets are formed in the aqueous PNIPAM homopolymer solution upon heating, the PNIPAM-*b*-PNVP block copolymer exists as the spherical droplet, spherical micelle, and single chain in hot water. When the PNIPAM homopolymer and the PNIPAM-*b*-PNVP block copolymer coexist in the aqueous solution, the spherical micelle and single chain components of the block copolymer are not affected by the coexistence of the homopolymer. Only the spherical droplet components of the

homopolymer and block copolymer are affected by mixing.

Figure IV-8 shows temperature dependences of the excess heat capacity ΔC_P at constant pressure (per monomer unit) for aqueous solutions of PNIPAM-*b*-PNVP block copolymer and PNIPAM homopolymer samples.[10] As well known, the thermogram for the aqueous PNIPAM homopolymer solution has a very sharp peak, revealing that the dehydration of the PNIPAM chain upon heating occurs cooperatively. However, the peak in the thermogram for the PNIPAM-*b*-PNVP block copolymer is much broader, indicating that the dehydration of the PNIPAM chain in the block copolymer takes place much gradually, may be due to the attachment of the hydrophilic PNVP block chain to a PNIPAM block chain end. It is well known that PNIPAM has a strong chain-end effect on the dehydration.[10]

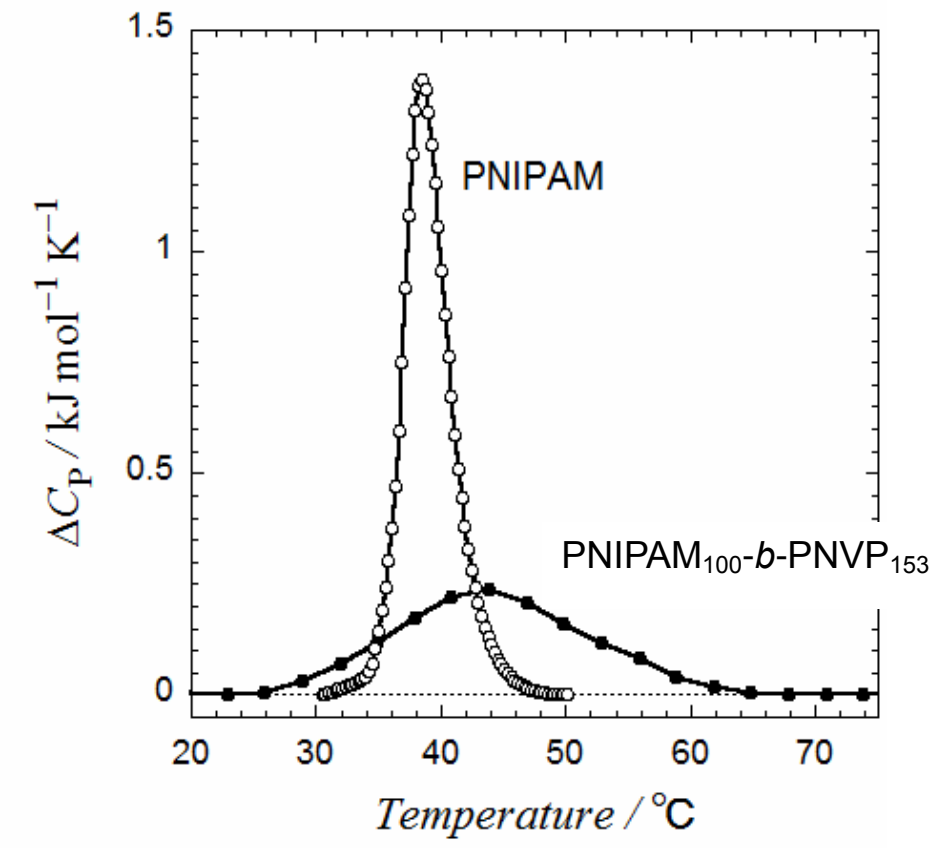

Figure IV-8. Endothermic curves of aqueous solutions of a PNIPAM homopolymer (unfilled circles) and $PNIPAM_{100}$-*b*-$PNVP_{153}$ block copolymer (filled circles).[11]

From these thermograms, we can say that the degree of hydration and then the hydrophobicity are considerably different between the PNIPAM homopolymer chain and PNIPAM block chain around 40-50 °C. Therefore, the PNIAPM homopolymer and block chains may not be miscible each other in that temperature range. Furthermore, as mentioned in Chapter II, the polymer-rich droplet of the PNIPAM homopolymer is frozen above ca. 35 °C, so that it may be difficult to incorporate the block copolymer chain even above 60 °C, where the PNIPAM block chain of the copolymer becomes also hydrophobic after the completion of dehydration. Thus, the PNIPAM homopolymer added to the block copolymer solution cannot control the competition between the micellization and liquid-liquid phase separation of PNIPAM-*b*-PNVP.

Although the polymer-rich droplet of the PNIPAM homopolymer is frozen, PNIPAM block chains of the copolymer may be adsorbed on the droplet surface to soften the surface by PNVP block chains of the copolymer. This softening can help the coalescence of the droplet, the formation of the network structure, and the shrinkage of the polymer-rich phase. Similar phenomena were reported for aqueous solutions of thermosensitive block copolymers.[4,5]

Reference

1. Riess, G. and Labbe, C. *Macromol. Rapid Commun* **2004**, *25*, 401-435.
2. Chausson, M.; Fluchère, A. S.; Landreau, E.; Aguni, Y.; Chevalier, Y.; Hamaide, T. *Int. J. Pharm*, **2008**, *362*,153-162.
3. Bijlard, A. C.; Wald, S.; Crespy, D.; Taden, A.; Wurm, F. R.; Landfester, K. *Adv. Mater. Interfaces* **2017**, *4*, 1600443.
4. Takahashi, R.; Sato, T.; Terao, K.; Qiu, X. -P.; Winnik, F. M. *Macromolecules* **2012,** *45*, 6111-6119.
5. Takahashi, R.; Qiu, X. P.; Xue, N.; Sato, T.; Terao, K.; Winnik, F. M. *Macromolecules*-**2014**, *47*, 6900-6910.
6. Sato, T.; Tanaka, K.; Toyokura, A.; Mori, R.; Takahashi, R.; Terao, K.; Yusa, S.

Macromolecules **2013**, *46*, 226−235.

7. Takahashi, R.; Sato, T.; Terao, K.; Yusa, S. *Macromoleues* **2015,** *48,* 7222−7229.
8. Tanaka, H. *Macromolecules* 1992, *25*, 6377-6380.
9. Sato, T.; Jinbo, Y.; Teramoto, A. *Polym. J*. **1999**, *31*, 285-292.
10. Qiu, X.; Koga, T.; Tanaka, F.; Winnik, F. M. *Sci. China Chem*. **2013**, *56*, 56–64
11. Y. Miyazaki, private communication.

Chapter V

Summary and Conclusions

This dissertation has dealt with the liquid-liquid phase separation and micellization occurring in aqueous solutions of a thermosensitive block copolymer poly(*N*-isopropyl-acrylamide)-*b*-poly(*N*-vinyl-2-pyrrolidone) (PNIPAM-*b*-PNVP), with and without the PNIPAM homopolymer upon heating. Here, the PNIPAM block chain becomes hydrophobic above ca. 30 °C, while the PNVP block chain is hydrophilic even at high temperatures.

Prior to study on the competition between micellization and liquid-liquid phase separation in aqueous solutions of PNIPAM-*b*-PNVP, Chapter II described small angle X-ray scattering (SAXS) measurements on aqueous solution of the PNIPAM homopolymer upon heating to investigate the liquid-liquid phase separation in the aqueous solution of the PNIPAM homopolymer. Below 29°C, the solution mostly contains the polymer single random coil chain with a minor scattering component of the loosely packed random coil. When the temperature reached to 31 °C and 33 °C, the liquid-liquid phase separation occurred, and the minor scattering component transfers to polydisperse spherical particles from the loosely packed random coil. As the temperature goes up to 35°C or higher, the main scattering component of the single random coil chain also transforms to spherical particles and there is no change in SAXS profiles between 35 °C to 73 °C. In addition, a tiny amount of globules of the PNIPAM chains coexist with spherical particles was also observed in the solution above 35°C. These findings indicate that the PNIPAM solution is not the thermodynamically equilibrium state in this temperature range.

Chapter III investigated the competition between the micellization and the liquid-liquid phase separation in aqueous solutions of the PNIPAM-*b*-PNVP samples with different PNIPAM

content *x* and total molecular weight upon heating by theory and SAXS measurements. SAXS profiles obtained were analyzed to determine the weight fractions of the spherical micelle, the spherical droplet, and the isolated chain in aqueous solutions of three PNIPAM-*b*-PNVP samples with different *x* as a functions of temperature. When *x* decreases, PNIPAM-*b*-PNVP prefers to form the spherical micelle rather than to form spherical droplets of the concentrated phase. Moreover, micellization and liquid-liquid phase separation temperatures increase with decreasing the degree of polymerization of the PNIPAM block chain. This SAXS result is consistent with the theoretical prediction based on the lattice model.

In Chapter IV, the PNIPAM homopolymer was mixed with the PNIPAM-b-PNVP block copolymer in aqueous solution. Upon heating, the liquid-liquid phase separation took place in the mixture solution, a network structure was observed in the phase-separating solution by optical microscopy, and the polymer-rich phase shrunk. Block copolymer single chains may be adsorbed on the polymer-rich droplet surface of the PNIPAM homopolymer to soften the surface and to help the coalescence of the droplet. The SAXS profiles obtained indicated that the phase separation of the PNIPAM homopolymer and the micellization of the PNIPAM-b-PNVP block copolymer occurred almost independently, probably because the degree of hydration and the hydrophobicity are considerably different between PNIPAM and PNIPAM-*b*-PNVP. Furthermore, because the PNIPAM homopolymer is frozen above ca. 35 °C, is may be difficult to incorporate with PNIPAM-*b*-PNVP at high temperatures, although the block copolymer chain may modify the surface of PNIPAM spherical particles.

List of Publications

1. Kuang, C.; Yusa, S. I.; Sato, T. Micellization and Phase Separation in Aqueous Solutions of Thermosensitive Block Copolymer Poly (*N*-isopropylacrylamide)-*b*-poly (*N*-vinyl-2-pyrrolidone) upon Heating. *Macromolecules*. **2019**, *52*, 4812-4819 (Chapter III).
2. Kuang, C.; Takahashi, R.; Sato, T. Phase Separation in Aqueous Solutions of Thermosensitive Polymer Poly(*N*‑isopropylacrylamide) upon Heating. *In preparation* (Chapter II).
3. Kuang, C.; Yusa, S. I.; and Sato, T. Phase Separation and Micellization in Aqueous Solutions of Mixtures of PNIPAM-*b*-Poly(*N*-vinyl-2-pyrrolidone) and PNIPAM Homopolymer upon Heating. *In preparation* (Chpater IV).

Related paper

1. Kuang, C.; Qavi, S.; Foudazi, R. Double-Stage Phase Separation in Dynamically Asymmetric Ternary Polymer Blends. *RSC Adv*, **2016**, *6*, 92104-92114.